Functionalisation of mica with (3-Aminopropyl)triethoxysilane: influence on imaging of extracellular vesicles from human cerebrospinal fluid by atomic force microscopy

Svetić, Ana

Master's thesis / Diplomski rad

2022

Degree Grantor / Ustanova koja je dodijelila akademski / stručni stupanj: **University of Rijeka / Sveučilište u Rijeci**

Permanent link / Trajna poveznica: https://urn.nsk.hr/urn:nbn:hr:193:235297

Rights / Prava: In copyright/Zaštićeno autorskim pravom.

Download date / Datum preuzimanja: **2024-05-18**

UNIVERSITY OF RIJEKA

DEPARTMENT OF BIOTECHNOLOGY

University Graduate Programme

Biotechnology in Medicine

Ana Svetić

Functionalisation of mica with (3-Aminopropyl)triethoxysilane: influence on imaging of extracellular vesicles from human cerebrospinal fluid by atomic force microscopy

Master´s thesis

Rijeka, 2022.

UNIVERSITY OF RIJEKA

DEPARTMENT OF BIOTECHNOLOGY

University Graduate Programme

Biotechnology in Medicine

Ana Svetić

Functionalisation of mica with (3-Aminopropyl)triethoxysilane: influence on imaging of extracellular vesicles from human cerebrospinal fluid by atomic force microscopy

Master´s thesis

Rijeka, 2022.

Mentor: Assoc. Prof. Mladenka Malenica

Co-mentor: Marko Perčić, PhD

SVEUČILIŠTE U RIJECI

ODJEL ZA BIOTEHNOLOGIJU

Diplomski sveučilišni studij

Biotehnologija u medicini

Ana Svetić

Funkcionalizacija tinjca 3-aminopropiltrietoksisilanom: utjecaj na vizualizaciju izvanstaničnih vezikula iz cerebrospinalne tekućine ljudi mikroskopijom atomskih sila

Diplomski rad

Rijeka, 2022.

Mentor: izv. prof. dr. sc. Mladenka Malenica

Komentor: dr. sc. Marko Perčić

Acknowledgments

First and foremost, I'd like to express utmost gratitude and thanks to my wonderful mentor, Assoc. Prof. Mladenka Malenica, for guidance and constant motivation in experimental and written work. Your energy is unparalleled, and I aspire to be like you one day.

Next, I'd like to thank co-mentor Marko Perčić, PhD, for his inexhaustible mentorship in all things technical – there's so much complex things to learn yet you make it sound so simple!

Lastly, I'd like to thank my better half and my family. For giving me hope, pushing me when it got hard and supporting me, always.

Without all of you, all of this would be impossible.

Mentor: Assoc. Prof. Mladenka Malenica

Co-mentor: Marko Perčić, PhD

Master´s thesis was defended on the **29.09.2022.** before the committee consisting of:

1. Assist. Prof. Ivan Gudelj, PhD, Department of Biotechnology

2. Assoc. Prof. Marin Tota, PhD, Faculty of Medicine

3. Marko Perčić, PhD, Faculty of Engineering (co-mentor)

4. Assoc. Prof. Mladenka Malenica, PhD, Faculty of Medicine (mentor)

The thesis has 54 pages, 22 figures and 34 references.

UNIRI
Sveučilište u Rijeci

CENTER FOR MICRO AND NANO
SCIENCES AND TECHNOLOGIES

Razvoj istraživačke infrastrukture na Kampusu Sveučilišta u Rijeci
OBRAZAC ZA IZVJEŠĆIVANJE O KORIŠTENJU ZNANSTVENE OPREME

Projekt Sveučilišta u Rijeci **„Razvoj istraživačke infrastrukture na Kampusu Sveučilišta u Rijeci"** financiran je iz Europskog fonda za regionalni razvoj (EFRR) u iznosu od 180.182.048,91 kn.

Vrsta rada:	Diplomski rad
Datum:	29.9.2022.
Institucija/e:	Medicinski fakultet Sveučilišta u Rijeci Centar za mikro- i nanoznanosti i tehnologije (NANORI) – Sveučilište u Rijeci
Naziv rada (HRV):	Funkcionalizacija tinjca 3-aminopropiltrietoksisilanom: utjecaj na vizualizaciju izvanstaničnih vezikula iz cerebrospinalne tekućine ljudi mikroskopijom atomskih sila
Naziv rada (ENG):	Functionalisation of mica with 3-aminopropyltriethoxysilane: influence on imaging of extracellular vesicles from human cerebrospinal fluid by atomic force microscopy
Sažetak:	Izvanstanične vezikule (IV) su nanočestice koje su prisutne u tjelesnim tekućinama ljudi uključujući i cerebrospinalnu tekućinu. Njihova vizualizacija se provodi elektronskom mikroskopijom i mikroskopijom atomskih sila, engl. Atomic Force Microscopy (AFM). AFM je napredna nano-tehnologija koja omogućava određivanje morfologije u nanometarskoj rezoluciji. Najčešći supstrat koji se koristi za vizualizaciju je tinjac međutim potrebna je njegova funkcionalizacija s ciljem jačeg vezivanje IV-a, pogotovo u zračnom modu AFM-a. 3-aminopropiltrietoksisilan (APTES) je amino-silanski linker koji se često koristi u funkcionalizaciji površina čijom adsorpcijom na površinu se povećava broj pozitivno nabijenih mjesta za vezanje IV-a. Time se poboljšava elektrostatska interakcija između negativno nabijene stanične membrane IV-a i pozitivno nabijene površine tinjca. Cilj rada je uspostaviti protokol funkcionalizacije tinjca s APTES-om i istražiti učinak vezivanja na vizualizaciju u zračnom modu AFM-a primjenjujući različite metode sušenja uzorka.
Ključne riječi (HRV):	izvanstanične vezikule, cerebrospinalna tekućina ljudi, mikroskopija atomskih sila, 3-aminopropiltrietoksisilan, 2,2-dimetoksipropan, sušenje pri kritičnoj točki, heksametildisilazan
Ključne riječi (ENG):	extracellular vesicles, human cerebrospinal fluid, atomic force microscopy, (3-Aminopropyl)triethoxysilane, 2,2-dimethoxypropane, critical point drying, hexamethyldisilazane
Autor rada:	Ana Svetić
Mentor/i:	Izv. prof. dr. sc. Mladenka Malenica
Komentor:	Dr. sc. Marko Perčić

Europska unija
Ulaganje u budućnost

STRUKTURNI I INVESTICIJSKI
FONDOVI

KONKURENTNA
HRVATSKA

Ministarstvo
znanosti,
obrazovanja
i sporta

Projekt je sufinancirala Europska unija iz Europskog fonda za regionalni razvoj.
Sadržaj ove publikacije isključiva je odgovornost Sveučilišta u Rijeci.

Summary

Extracellular vesicles (EV) are nanoparticles that are present in biofluids, including human cerebrospinal fluid (CSF). Their visualisation is performed by Electronic Microscopy (EM) and atomic force microscopy (AFM). AFM is advanced nanotechnology that enables the determination of morphology in nanometer resolution. The most common substrate used for visualisation is mica, however, its functionalisation is needed with the aim of stronger binding of EVs, especially in the AFM air mode. (3-Aminopropyl)triethoxysilane (APTES) is an amino silane linker that is often used in the functionalisation of surfaces, whose adsorption on the surface increases the number of positively charged sites for EV binding. Functionalisation improves the electrostatic interaction between the negatively charged EV cell membrane and the positively charged surface of the mica. The aim of the work is to establish a protocol for the functionalisation of mica with APTES and to investigate the effect of binding on visualisation in the air mode of AFM by applying different methods for dehydration and drying of the sample. Treatment of EVs before their visualisation included: fixation with paraformaldehyde (PFA, 3 %) and glutaraldehyde (GA, 1.5 %), dehydration with ethanol or 2,2-dimethoxypropane (2,2-DMP) and drying at either critical point of CO_2 (CPD) or with hexamethyldisilazane (HMDS). The most optimal sample preparation protocol for visualisation is the one that involves functionalisation of mica by APTES in vapour, dehydration with 2,2-DMP and HMDS drying. This protocol showed the best overlap in total detected EVs according to diameter and height, highest diameter median and mean and lowest number of outliers out of all other protocols. The detected shapes of EVs were round, "cup-shaped" and multilobed. Future research should focus on methods that can differentiate EVs from other particles of the same outward appearance, like immuno-based interaction of EV antigens with antibodies.

Sažetak

Izvanstanične vezikule (IV) su nanočestice koje su prisutne u tjelesnim tekućinama uključujući i cerebrospinalnu tekućinu ljudi. Njihova vizualizacija se provodi elektronskom mikroskopijom i mikroskopijom atomskih sila, engl. Atomic Force Microscopy (AFM). AFM je napredna nano-tehnologija koja omogućava vizualizaciju morfologije u nanometarskoj rezoluciji. Najčešći supstrat koji se koristi za vizualizaciju je tinjac međutim potrebna je njegova funkcionalizacija s ciljem jačeg vezivanje IV-a, pogotovo u zračnom modu AFM-a. 3-aminopropiltrietoksisilan (APTES) je amino-silanski linker koji se često koristi u funkcionalizaciji površina, a čijom adsorpcijom na površinu se povećava broj pozitivno nabijenih mjesta za vezanje IV-a. Time se poboljšava elektrostatska interakcija između negativno nabijene stanične membrane IV-a i pozitivno nabijene površine tinjca. Cilj rada je uspostaviti protokol funkcionalizacije tinjca s APTES-om i istražiti učinak vezivanja na vizualizaciju u zračnom modu AFM-a primjenjujući različite metode sušenja uzorka. Prije vizualizacije IV-e su fiksirane otopinom paraformaldehida (PFA, 3 %) i glutaraldehida (GA, 1.5 %), dehidrirane etanolom ili 2,2-dimetoksipropanom (2,2-DMP) i osušene pri kritičnoj točki CO_2 ili heksametildisilazanom (HMDS). Optimalni protokol pripreme uzorka za vizualizaciju uključuje: fukcionalizaciju tinjca isparavanjem APTES-a, dehidraciju sa 2,2-DMP-om i sušenje HMDS-om. Ovaj protokol je pokazao najbolje preklapanje promjera i visine po ukupnom broju IV-a, najveći medijan promjera i srednju vrijednost te najmanji broj čestica koje odstupaju u usporedbi s ostalim protokolima. Detektirane čestice bile su okruglog, višerežnjastog i konkavnog oblika. Budući da su ove metode usredotočene na otkrivanje IV-a prema njihovom obliku, promjeru i visini, naredna istraživanja trebala bi se usredotočiti na metode koje mogu razlikovati IV-e od drugih čestica istog ili sličnog vanjskog izgleda, primjerice imunointerakcija antigena IV-a s protutijelima.

Contents

1. INTRODUCTION

1.1. Extracellular vesicles: General Properties

Extracellular vesicles (EVs) are nanosized, membranous structures (Figure 1.) that are secreted from almost every cell and are present in most human biofluids e.g., blood, urine, saliva, tears, milk and cerebrospinal fluid (CSF) (1–3). Upon their release, EVs are used as vehicles for cargo molecules such as proteins and genetic material (1). They can transfer macromolecules via highly advanced system of intercellular communication (4), who's mechanism is not yet clear. Furthermore, it has been discovered that EV composition reflects the state of its parental tissue (2) - a fact that has amassed a considerable amount of attention from the scientific community, giving EVs immense potential for future application in nanomedicine, treatments and diagnostics (3). EVs are highly heterogeneous, with size distribution varying from 30 – 2000 nm (4) and their classification is still a complicated matter. They can be divided into subclasses, such as: exosomes, microvesicles and additionally apoptotic bodies based on their size, protein markers and other features (5).
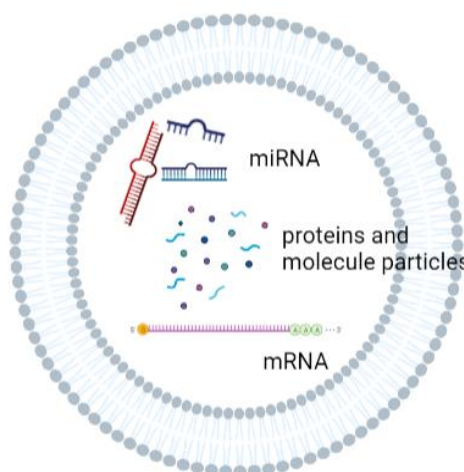
Figure 1. Extracellular vesicle and its inner contents. Image created in BioRender (BioRender, Toronto, Ontario, Canada) (6).

1.2. EV imaging: Atomic Force Microscopy

To visualise and characterise morphology of EVs, advanced and optimised microscopy methods are required (2). The International Society of Extracellular Vesicles (ISEV) currently recommends electron microscopy (EM) and atomic force microscopy (AFM) as the main high-resolution imaging techniques to assess sample heterogeneity and EV morphological properties (3). Both EM and AFM are low-throughput techniques, since they allow only several particles to be observed at a time, and they give detailed information on the size, shape, and morphology of EVs. In addition, biomechanical and biophysical characteristics like adhesion, stiffness, density or elastic properties can be obtained with AFM (2). Invented by Binnig, Quate and Gerber in 1985 (7) (Figure 2.), one of the most attractive aspects of AFM is its accuracy, high-resolution and the ability to measure and image a sample in a non-destructive way.
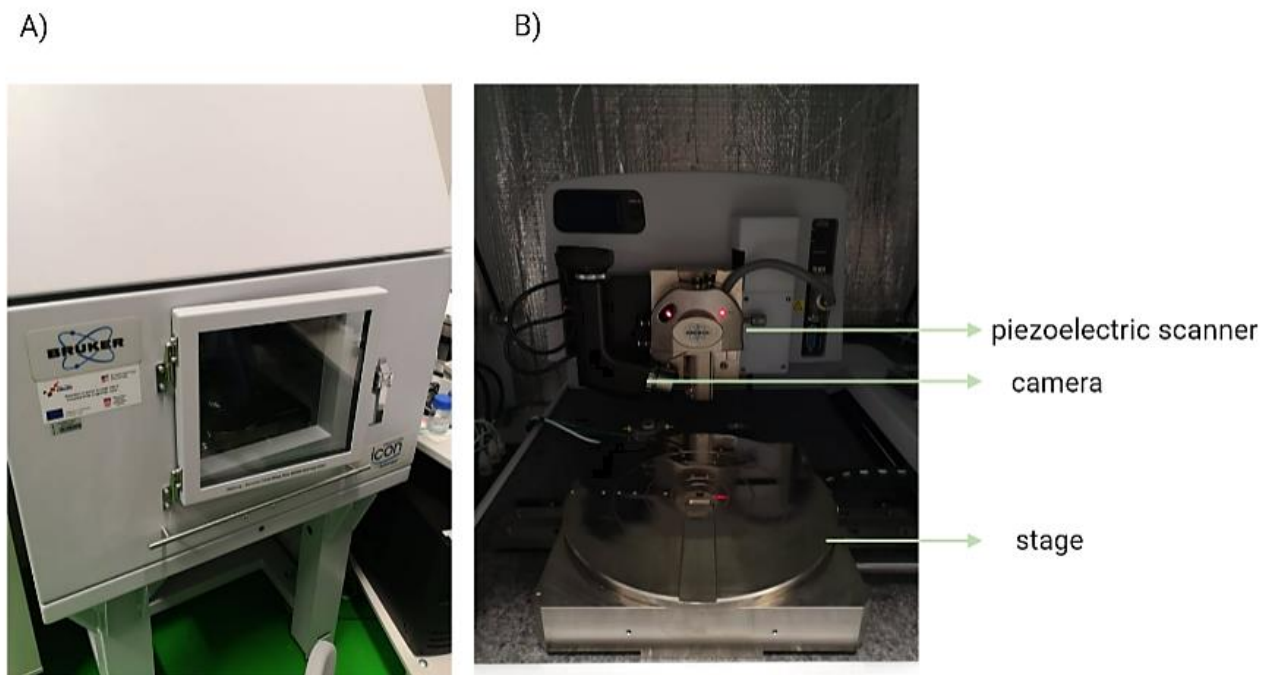
Figure 2. Atomic force microscope, Dimension Icon (Bruker, MA, USA) in the Center for micro- and nanosciences and technologies, University of Rijeka. Outer "box" configuration which protects the microscope from vibrations and other environmental factors (A); inner configuration with a stage, piezoelectric scanner and a camera (B).

1.2.1. Atomic Force Microscopy: Basic Operation Principle

AFM operates by using an extremely sharp, nano-sized tip that's attached to an oscillating cantilever on its free end. The tip and cantilever are often referred to as the probe, which scans the sample surface in a raster-like motion (Figure 3.A). During the scanning, the probe is controlled by a piezoelectric scanner that controls its lateral and vertical position (7) (Figure 3.B). As the tip moves over the changing surface topography of the sample, the deflection of the cantilever changes. Change in the deflection is caught by a laser beam (Figure 3.C), positioned on the backside of the cantilever, and directed to a four-quadrant position sensitive photodiode (PSPD) (Figure 3.D). PSPD then converts the received light signal from the laser beam to computer-readable voltage (8). All the information gathered by the computer is then combined to generate a topographic image of the surface in three dimensions. Feedback loop controls the vertical extension of the piezoelectric scanner (7) and ensures that the image mapping is as close to the sample surface.

Figure 3. AFM basic operation principle schematic: AFM probe (A); piezoelectric scanner (B); reflected laser beam (C) caught by the photodiode (D). Picture retrieved and modified from (7).

1.2.2. Atomic Force Microscopy: Techniques and Modes of Operation

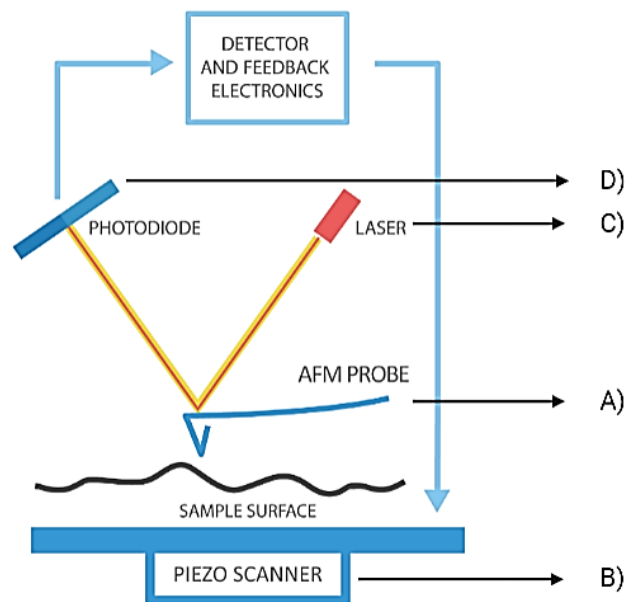EVs can be imaged in both air and liquid. The most prominent difference between EM and AFM is that the AFM imaging is done in different mediums (air, liquid) and the fact that liquid technique is much more complicated to operate than air technique. A crucial parameter for successful imaging is the selection of the appropriate mode of operation (2). There are several modes: contact (Figure 4.A), intermittent contact (mostly known as tapping) (Figure 4.B) and non-contact (Figure 4.C). Briefly, in contact mode, the tip contacts the surface through the adsorbed fluid layer on the sample surface. The detector monitors the changing cantilever deflection, and the force is calculated using Hooke's law (1) (9),

$$F = - k \times x \tag{1}$$

where F = force, k = spring constant, x = cantilever deflection. The spring constant needs to be relatively low to avoid damage of a biological sample (10). The feedback circuit then adjusts the probe height aiming to maintain a constant force and deflection on the cantilever (9). In tapping mode, the cantilever oscillates at or slightly below its resonant frequency and the tip lightly taps on the sample surface during scanning (9), creating intermittent contact. Lastly, in non-contact mode (a dynamic AFM technique) the cantilever oscillates above its resonant frequency (9), near the surface but never touching it.
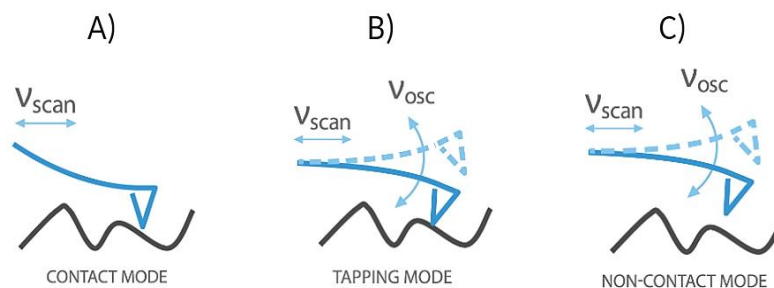
Figure 4. AFM modes of operation: contact mode (A), tapping mode (B) and non-contact mode (C). V_{scan} represents scanning frequency, V_{osc} represents oscillation frequency. Picture retrieved from (7).

1.3. Sample Preparation for Atomic Force Microscopy Imaging in Air

Before imaging by AFM in air, biological sample must be immobilised via fixation. That way, the components and structures of the dynamic biological system are preserved and kept as much as possible in their native state. Most commonly used chemical fixatives are aldehydes – glutaraldehyde (GA) and paraformaldehyde (PFA) - that form cross-links. GA (molecular formula: $C_5H_8O_2$, molecular weight: 100.11 g/mol) is a well-known, linear 5-carbon dialdehyde that is often used in biomedical sciences (Figure 5.A). The principle behind the fixation is the reaction between glutaraldehyde and amine groups of the nucleophiles, such as proteins, that happens around neutral pH, cross-linking the protein and maintaining the stable structure. PFA (molecular formula: $OH(CH_2O)nH(n=8-100)$, molecular weight: 30.026 g/mol) is a polyoxymethylene (Figure 5.B), polyacetal molecule that is smaller than GA and therefore penetrates faster. However, GA is faster in cross-linking proteins since reaction can occur through both –CHO groups and over greater distances (11). Differences between GA and PFA bring their own advantages (12). Using a combination of PFA:GA mixture immobilises samples onto the surface by creating covalent bonds between proteins (12).

A)   B)
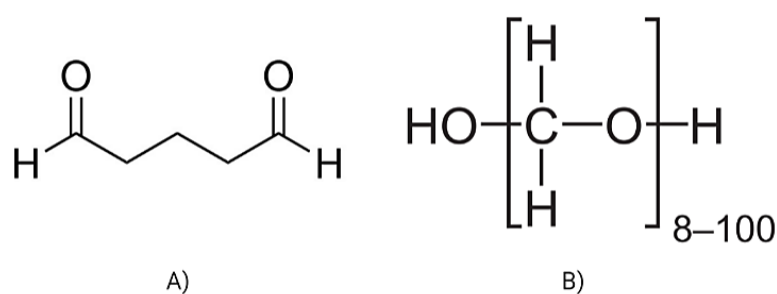
Figure 5. Fixative GA (A) and PFA (B) molecules. Presentation done in MarvinSketch (Chemaxon, Budapest, Hugary).

1.4. Functionalisation of Mica

Mica is a natural stone formed as multiple distinct layers (13). It has a large atomic flat surface, and it can be easily prepared. When freshly cleaved, surface root mean square of mica stubs is 0.06±0,01 nm (14), which makes it a good substrate for AFM. EVs usually display negative surface potential, which is a problem since mica has a negative net charge. Functionalisation of mica with aminosilanes for AFM imaging was first proposed by Lyubchenko et al. (15) using (3-aminopropyl)triethoxysilane (Figure 6.A), otherwise referred to as APTES (molecular formula: $C_9H_{23}NO_3Si$, molecular weight: 221.37 g/mol), to produce a positively charged substrate; APTES-mica (16). APTES is a commonly used organosilane for surface functionalisation of silicon oxide surfaces. It has an amino group that makes a homogenous layer on the support substrate and reverses the mica surface charge through protonated amino groups at neutral pH (14). The purpose of functionalisation is, therefore, to make the mica charge less negative so the vesicles bind better (Figure 6.B). In addition to pure APTES functionalisation, fixatives such as glutaraldehyde or paraformaldehyde can be used to further immobilise the vesicles on the surface (Figure 6.C).

Figure 6. Schematic of (3-Aminopropyl)triethoxysilane (APTES) (A); APTES deposited onto mica surface (B); APTES with additional glutaraldehyde (GA) and an extracellular vesicle (C). (A) retrieved from (17), (B) retrieved from (18) and modified in BioRender.

1.5. Sample Dehydration and Drying

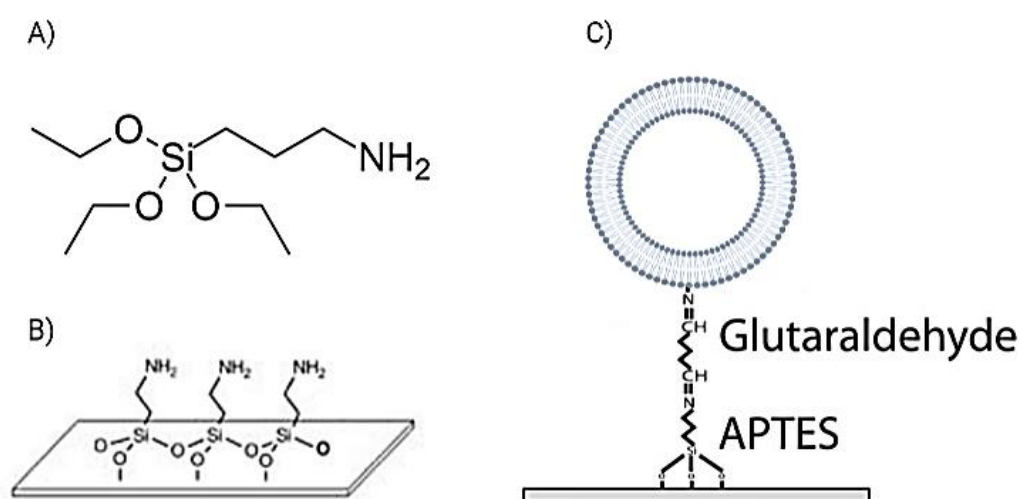AFM in air environment requires samples to be properly dried before imaging. There are generally three types of drying methods used for biological samples: air drying, drying at critical point (CPD) and drying by hexamethyldisilazane (HMDS), that are usually performed after dehydration. Dehydration is a natural step that follows the fixation, replacing the aqueous content of the sample with an organic solvent such as ethanol (EtOH) or acetone. The concentration of organic solvent is slowly increased until all the water from the sample is replaced with the organic solvent (11). This step is done because of the water's high surface tension. Replacing the water with organic solvents greatly reduces that surface tension and ensures less further damage to the sample.

1.5.1. Air Drying

The easiest drying technique, which leaves a dehydrated sample to dry on air at room temperature until all solvent evaporates (11). However, the downside of the simplicity is the shrinkage and collapse of the sample structure due to high surface tension of water (around 0.07 N/m), despite sample being immobilised by fixation (2).

1.5.2. Drying at Critical Point of CO_2

CPD is an established drying method for biological tissue, first introduced commercially for Scanning Electron Microscopy (SEM) specimen preparation by Polaron (Quorum Technologies, Newhaven, East Sussex, UK) in 1971. (19). It relies on a physical principle called critical temperature and its corresponding pressure, a boundary between phases of liquid and vapour where they can co-exist and therefore have the same density (Figure 7.). This boundary makes it possible to remove fluids from the sample in a vapour phase, at the same time avoiding damaging the biological tissue. First, the water from a sample is replaced with a suitable inert fluid of lower surface tension. Commonly used are methanol, EtOH, amyl acetate and acetone (19). After replacing the water with previously mentioned organic solvent in gradient, organic solvents are then exchanged with liquid CO_2. By raising the temperature from +5 °C to +35 °C and the

pressure up to 8622757.5 Pa in the chamber, CO_2 is released from the chamber and sample is left dried and intact (11).

1.5.3. Hexamethyldisilazane Drying

Good alternative for the CPD method is drying by HMDS (Figure 8.) - a rapid technique which uses minimal equipment. HMDS, also known as bis(trimethylsilyl)amine (molecular formula: $[(CH_3)_3Si]_2NH$, molecular weight: 161.39 g/mol) cross-links proteins, therefore adding strength to the sample during air drying (21) and has low surface tension that enables it to evaporate from a sample with minimal distortion (11). The true mechanism of the reaction is not yet known.
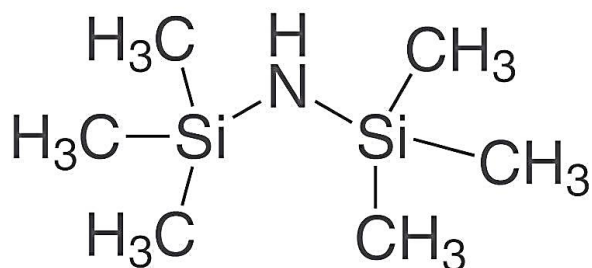
2. THE GOAL OF THE THESIS

The aim of this study was to optimise sample preparation protocol for EV visualisation by AFM in air that involves functionalisation of mica with APTES, different dehydration, and drying methods.

The specific aims of this thesis were:

1. To determine the difference in mica functionalisation with APTES when applied in liquid or by evaporation method, through roughness values and introduction of artifacts;
2. To establish how APTES impacts binding of EVs to mica;
3. To determine which dehydration and drying method gives better yields in bound EVs;
4. To compare the EV size and height distribution using a statistical test.

3. MATERIALS AND METHODS

3.1. Sample Collection

The sample used in this work was cerebrospinal fluid (CSF), collected from patients with traumatic brain injury (TBI) at Clinical Hospital Centre Pula (Pula, Croatia). Patients received ventriculostomy; a surgical procedure involving the placement of a catheter that connects the ventricles of the brain to an external collecting device (23). For all the samples the informed consent and an approval given by a family member was obtained. The study was conducted according to the guidelines of the Declaration of Helsinki, and approved by Ethics Committee of General Hospital Pula, Pula, Croatia (Number: URBr 4943/10-1, 17 July 2019). EVs were isolated by size-exclusion chromatography from the pool of CSF of TBI patients which was not part of this work.

3.2. Sample Preparation for Atomic Force Microscopy Imaging

3.2.1. Functionalisation of the Mica

Mica grade V-1 12mm diameter x 0.15 mm thick (Structure Probe, Inc., West Chester, PA, USA) was freshly cleaved with adhesive tape by pressing the top of the mica on the sticky end of the tape while simultaneously holding it with tweezers. After removing the top layer of mica, top of the surface was marked by scratching.

3.2.2. (3-Aminopropyl)triethoxysilane Liquid Deposition Method

2 µL of 99% APTES (Sigma-Aldrich, St. Louis, MO, USA) was first dissolved in 10 mL HiPerSolv CHROMANORM® water for HPLC (VWR International, Radnor, PA, USA). That way, the Si-OR bonds of APTES hydrolyse with water to form silanol Si-OH groups (Figure 9.)(24).
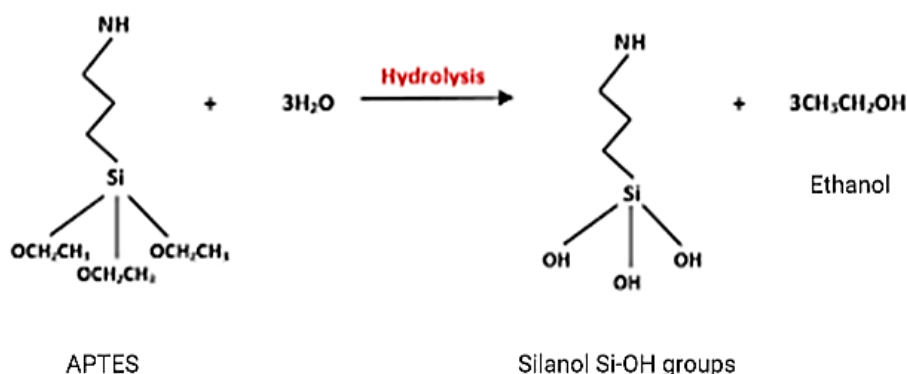
Figure 9. APTES hydrolysis. Si-OR bonds of APTES hydrolyse with water to form silanol Si-OH groups. Obtained from (24).

Dissolved, 0.02% APTES solution was filtered into an Eppendorf tube. Next, 100 µL of 0.02% APTES solution was deposited onto freshly cleaved mica and incubated for three minutes in a moist chamber (25). After incubation, APTES was removed by adding 200 µL of HiPerSolv water onto the mica and pipetted out. Functionalised surface was then thoroughly washed three times with 200 µL of HiPerSolv water, and then also three times with 200 µL of PBS (D-PBS, Formula III Phosphate Buffer Saline 1 LT, Electron Microscopy Sciences Inc., Hatfield, PA, USA). Sample was then immediately added and further processed.

3.2.3. (3-Aminopropyl)triethoxysilane Vapour Deposition Method

The desiccator was flooded with gas nitrogen for five minutes (26). 30 µL of filtered 0.02% APTES and 10 µL of 99.6% triethylamine (VWR International, Radnor, PA, USA) were separately pipetted in a Petri dish (never mixed throughout the process), after which the Petri dish was placed under the hood of an empty, nitrogen flooded desiccator. Triethylamine is necessary for efficient APTES layer formation. Freshly cleaved mica was also placed in the same Petri dish and into the same desiccator. The desiccator was closed and left undisturbed overnight. The next day functionalised mica and the chemicals were removed from the desiccator,

which was then flooded with nitrogen gas for five minutes. Functionalised mica was stored in another, well-sealed desiccator until further processing (Figure 10.).

Figure 10. Functionalised mica stored in a desiccator.

3.2.4. Sample Preparation

The EVs, isolated by size-exclusion chromatography from CSF of TBI patients, were defrosted on ice for 10 minutes. Fixation was performed using PFA:GA (6 %:3% in phosphate buffer) solution in 1:1 (v/v) with the EVs in Eppendorf tube (final concentration of fixative was 3% PFA : 1.5% GA in phosphate buffer) (12). 32% PFA aqueous solution was acquired from Electron Microscopy Sciences (Hatfield, PA, USA) while 25% GA aqueous solution was obtained from Structure Probe Inc. (West Chester, PA, USA). 50 µL of fixated sample was added onto the dried APTES-mica, left to incubate for 30 minutes in a closed Petri dish. Afterwards, surface was rinsed with PBS three times and then with water three times.

3.3. Sample Dehydration and Drying

There were two methods for dehydration and drying explored: dehydration in EtOH gradient - drying at critical point of CO_2 and dehydration with 2,2-dimethoxypropane (2,2-DMP) - drying with HMDS.

3.4. Ethanol Dehydration and Drying at Critical Point of CO_2
3.4.1. Ethanol Dehydration

Gradient was achieved by preparing serial EtOH dilutions (30%, 50%, 70%, 80%, 90% and finally, 99%) using HiPerSolv CHROMANORM® water and absolute EtOH (Gram-Mol, Zagreb, Croatia) (Figure 11.). 1 mL of each dilution was pipetted separately on a 12-well plate (Figure 11.). APTES-mica with the sample was first immersed into 1 mL of 30% gradient solution, then the rest of the dilutions up to 100% EtOH, with 10 minutes of incubation in each well (11,21). The sample was left in the 100% EtOH well until CPD.
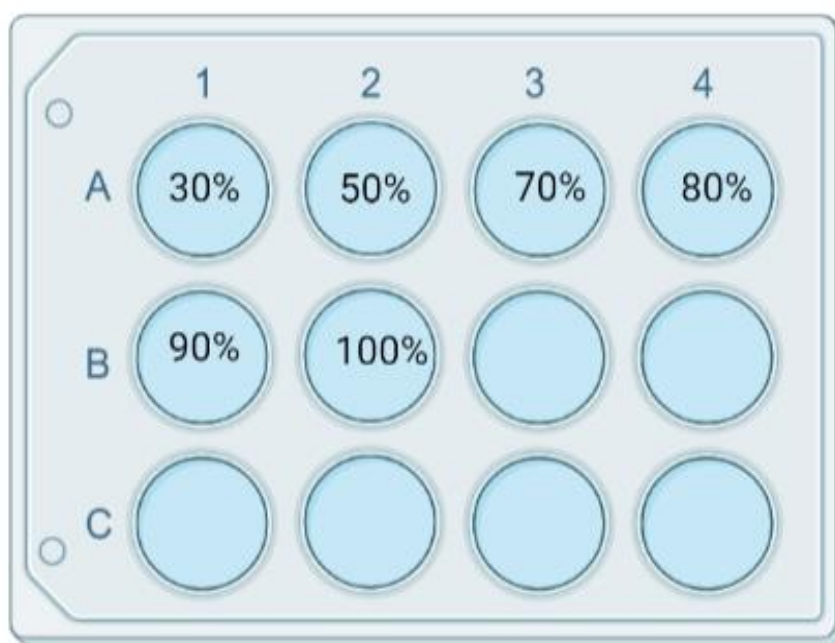
Figure 11. EtOH dehydration protocol. Functionalised APTES-mica samples were immersed in wells of EtOH gradient solutions (30%, 50%, 70%, 80%, 90% and 100%), 10 minutes. Image created in BioRender.

3.4.2. Drying at Critical Point of CO₂

Drying method was performed on K850 Critical Point Dryer (Quorum Technologies Ltd., Lewes, UK) (Figure 12.A). After pre-cooling the chamber on +5 °C, dehydrated APTES-mica were loaded into a specialised EK4130 bulk holder (Figure 12.B). The entire contraption was then loaded onto the depressurised chamber and liquid CO_2 was added to the top of the upper red line on the view window (Figure 12.C). Samples were then soaked in CO_2 with a stirrer for 3 minutes, on +5 °C and the chamber was purged whilst maintaining meniscus between the upper and lower red line. Soaking and purging was performed 3 times aiming to replace EtOH with liquid CO_2. Afterwards, the chamber was filled to the top of the upper red line and the heater was turned on. Stable conditions of +35 °C and 8622757.5 Pa were maintained for 35 minutes in order to reach the CO_2 critical point. At the critical point, liquid and gas CO_2 phases are in equilibrium with no surface tension, which results in release of CO_2 from the chamber. Then the system was depressurised for 20 minutes, and sample was dried.

A)   B)   C)
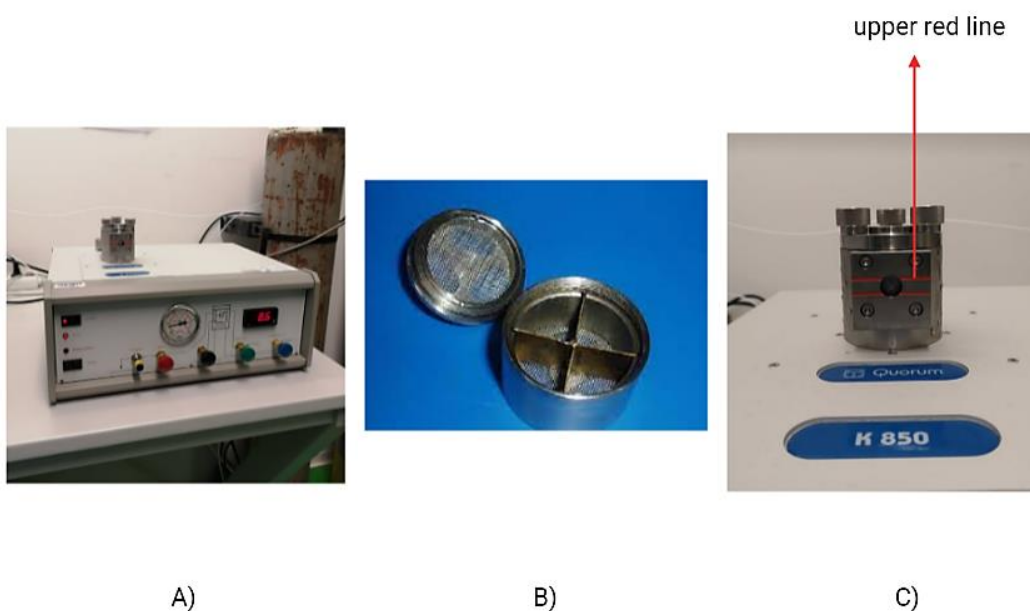
Figure 12. Quorum K850 Critical point dryer (Quorum Technologies Ltd, Lewes, UK) in the joint laboratory of Department of Physics and Centre for micro- and nanosciences and technologies, NANORI, University of Rijeka (A); EK4130 bulk holder, picture courtesy of Quorum Technologies Ltd. (B); view window with lower and marked upper red line (C).

3.5. 2,2-Dimethoxypropane Dehydration and Hexamethyldisilazane Drying

3.5.1. 2,2-Dimethoxypropane Dehydration

Dehydration was performed with 98% 2,2-DMP (Alfa Aesar, Haverhill, MA, USA). 2,2-DMP reacts with water in presence of hydrogen atoms and produces methanol and acetone in an endothermic reaction. Both are considered as dehydrating, with acetone being highly volatile. Therefore, it's crucial to make sure that all the bottles and dishes with acetone are firmly closed. Dehydrating solution was prepared by adding 5 µL of concentrated HCl (Kemika, Zagreb, Croatia) into 5 mL of 98% 2,2-DMP. 1 mL of the solution was needed to cover the bottom of the glass Petri dish, in which sample (APTES-mica with the EVs) was immersed. The sample was incubated for 10 minutes, after which the solution was removed from the glass Petri dish and the process was repeated 2 more times with 100% acetone. The sample was left in 100% acetone to prevent drying, and the glass Petri dish firmly closed and wrapped with parafilm until drying.

3.5.2. Hexamethyldisilazane Drying

Using this drying technique, acetone is effectively replaced with HMDS (Sigma-Aldrich, MO, USA) in a gradient fashion, starting with 100% acetone solution, then 75% acetone:25% HMDS solution, 25% acetone:75% HMDS solution and finally 100% HMDS solution. All samples were soaked for 15 minutes in each solution except for the last one (100% HMDS) where the sample was kept in for 20 minutes. Afterwards, samples were removed into a dry Petri dish, dried with wipes by touching of the edge and placed into a desiccator overnight, until imaging.

4. Atomic Force Microscopy Imaging

AFM imaging was performed in air tapping mode on a Dimension Icon AFM (Bruker Corporation, MA, USA). Samples were carefully transferred from the desiccator onto a modified sample "stage" with added adhesive tape so the mica crystals wouldn't move during imaging. Samples were marked with their respective code-numbers before the imaging process was started. Two images, 10x10 µm in size, were taken of each sample and

they were cropped to 5x5 μm. Two particles of particular interest, from representative 5x5 μm image, were cropped out and shown separately (*See Section 4.*). There were also 1x1 μm control images: mica (Control A), APTES-mica liquid deposition (Control B), APTES-mica vapour deposition (Control C), APTES-mica liquid deposition + PFA:GA (3%:1.5%) (Control D), APTES-mica vapour deposition + PFA:GA (3%:1.5%) (Control E). The images were obtained using silicon nitride SCANASYST-AIR probes (Bruker Corporation, MA, USA) (Figure 13.A). Triangular in size, their tip radius varies from 2 - 12 nm while their maximum resonant frequency goes up to 95 KHz and spring constant up to 0.8 N/m. The probes are placed on the cantilever stand before being placed into an AFM (Figure 13.B).
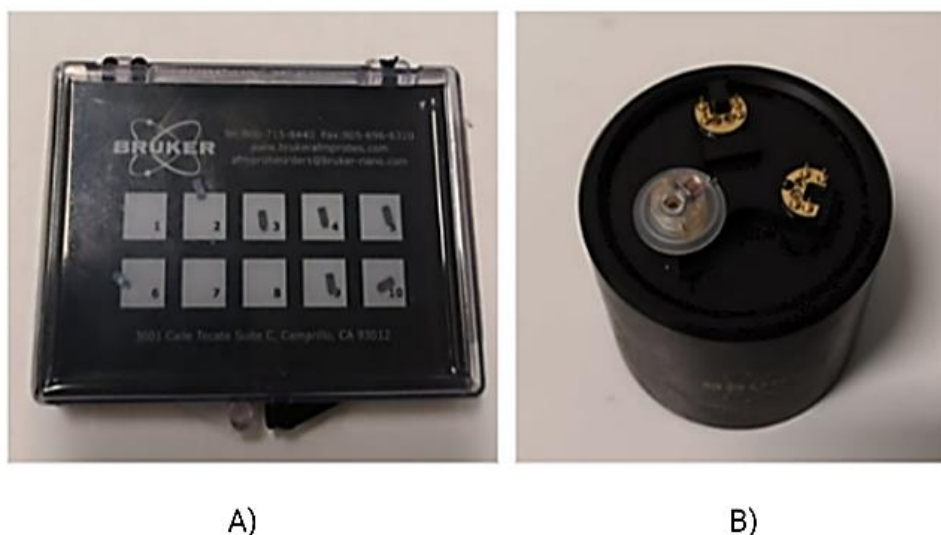
Figure 13. Bruker silicon nitride SCANASYST-AIR probes (A), Dimension Icon heater-cooler cantilever stand (B).

4.1. Image Analysis: Gwyddion

Gwyddion 2.60 (version released on 12th of November 2021) is a free, modular, multiplatform, open-source software for scanning probe microscopy (SPM) data processing (Czech Metrology Institute, Czech Republic). Its main task is to provide fast and reproducible data-processing routines (27). Firstly, the dimensions of the tip radius were determined by using the JEOL Field Emission (JSM-7800F) image of the tip (Figure 14.) and the *Measure distances and directions between points* tools. Two

approximate lines were drawn over edge of the tip (horizontally) and next to it (vertically), determining the dimensions of the said tip to be 6.5 nm in both width and height.
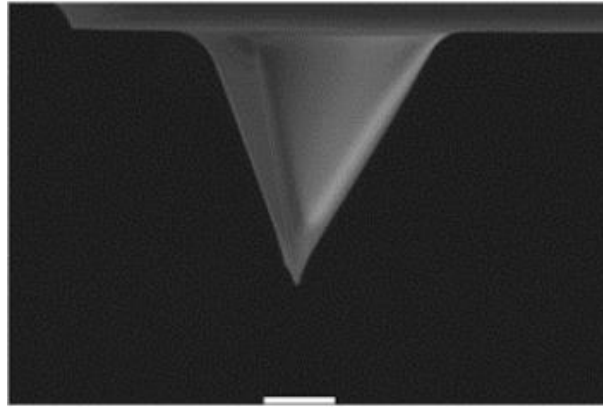
Figure 14. Scanning electron microscope (JEOL Field Emission JSM-7800F, Tokyo, Japan) image of SCANASYST-AIR cantilever (Bruker Corporation, Billerica, MA, USA) 1μm in size. Courtesy of joint laboratory of Department of Physics and Centre for micro- and nanosciences and technologies, NANORI, University of Rijeka. White bar 1 μm.

Next, two images, 10x10 μm in size, were processed following the Skliar et al. (28) but with modification of skipping the surface reconstruction step. *Plane Level* was used to remove the tilt in the substrate from the scan data, *Align Rows* to correct the various artefacts made during the scanning of the mica surface, *Remove Scars* to remove common scar errors made during scanning, *Flatten Base* to align the mica surface at the zero height (Z axis to zero). When the surface was processed, *Mark by Threshold* was used to mark EVs on the scanned surface (28). The selected threshold for each sample varied from 1.5 - 2.8 nm, depending on background noise. Following the procedure above, the two 10x10 μm images were cropped using *Crop* tool, creating 5x5 μm images. One representative 5x5 μm image was presented with two typical particle shapes, cropped from this image. From 10x10 μm images, raw data characterizations of *Maximum Martin diameter* and *Height* were exported and plotted against particle count in Microsoft Excel, using the available *Distributions* algorithms in the *Grains*

menu. Additionally, *Row/Column Statistics* and *Statistical Quantities* were used to compute basic statistical quantities from a selected masked area. The results of the calculations were R_a (2) and R_q (3). R_q is the value of the height irregularities that's computed from data variance more commonly known as root mean square, and R_a is the standard roughness parameter otherwise known as roughness average (Figure 15.).

$$Ra = \frac{1}{l_r} \int_0^{l_r} |z(x)| \, dx \qquad (2)$$

$$Rq = \sqrt{\frac{1}{l_r} \int_0^{l_r} z(x)^2 \, dx} \qquad (3)$$

R_q = root mean square

R_a = roughness average

$z(x)$ = 2D surface height

l_r = length of the sample
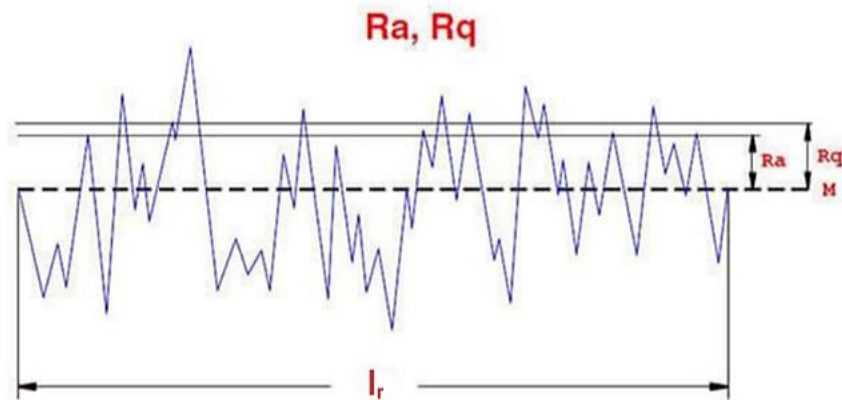
Figure 15. R_q and R_a, visualised on 2D plane of a sample length l_r Obtained from (29).

From R_a, basic properties of the height values distribution (variance, skewness, kurtosis) can be calculated. Unlike R_a, they are 3D characteristics with parameters for the whole surface: S_q (4) and S_a (5). S_q is a mean square roughness of height irregularities (otherwise known as root mean square of height, RMS_{height}) whilst S_a represents mean roughness of height irregularities (arithmetic mean of height, extension of R_a).

$$s_q = \sqrt{\frac{1}{A} \int \int_A z^2(x,y)\, dx\, dy} \quad (4)$$

$$S_a = \frac{1}{A} \int \int_A |z(x,y)|\, dx\, dy \quad (5)$$

S_q = root mean square of height

S_a = arithmetic mean of height

z(x,y) = 3D surface height

A = sample surface

Controls (Control A, B, C, D, E) were processed following the same protocol. What's specific is that *Roughness* tool was used to evaluate 2D and 3D parameters of control surfaces. All control images were styled in a Gwyddion.net coloring mode.

5. Statistical analysis

The analysis was performed in Microsoft Excel 2010 (Microsoft Corp., WA, USA). Data distribution was downloaded in .csv format from Gwyddion software and tested using Data Analysis Toolpack. Origin Software (OriginLab Corp., MA, USA) was used to perform descriptive analysis, Kolmogorov-Smirnov normality test (significance level: α=0.05) for diameter and height data, Kruskal-Wallis H-test (also known as nonparametric ordinary one-way ANOVA test) with a post-hoc Mann-Whitney U-test for diameter values, and parametric ANOVA test with post-hoc Mann-Whitney U-test for height values. Criteria of statistical significance was considered p ≤ 0.05.

4. RESULTS

4.1. Impact of Mica Functionalisation With (3-Aminopropyl)triethoxysilane On the Surface Roughness

First task was to visualise the surfaces of bare mica (Control A), mica functionalised with APTES using liquid (Control B) and vapour (Control C) deposition technique, and finally mica functionalised with APTES with addition of PFA:GA (3%:1.5% dissolved in PBS) fixatives using liquid (Control D) and vapour (Control E) deposition technique. The roughness values were calculated using 1x1 μm image in size and presented in Table 1. The values of maximum height obtained for Control A (Figure 16.A) was ~4 nm, Control B (Figure 16.B) was 19 – 21 nm and Control C (Figure 16.C) was ~6 nm. When it comes to Control D and E, Control D (Figure 16.D) has no apparent impurities and the maximum surface height of 12 nm, whilst Control E (Figure 16.E) is showing slight impurities in the form of peaks that are bouncing off of normal surface height (~5.6 nm).
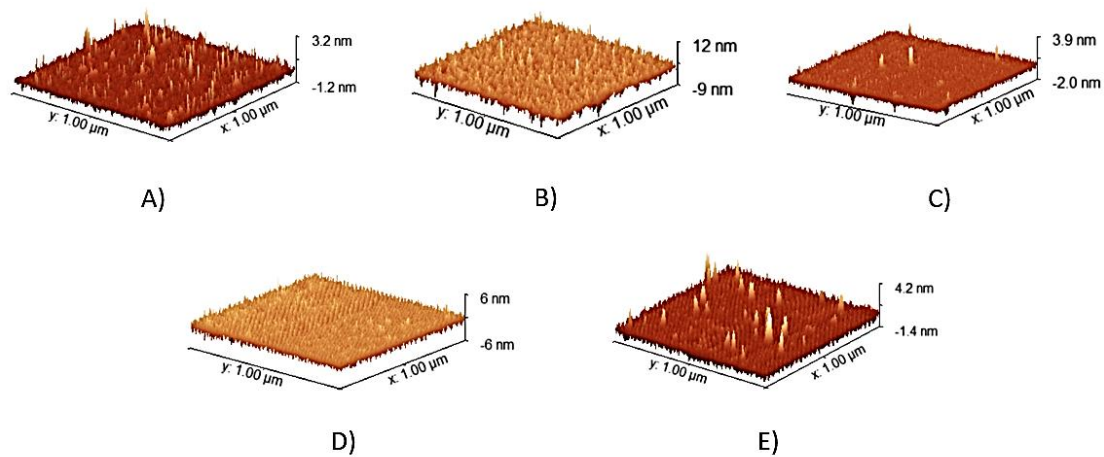
Figure 16. 3D images of surfaces obtained by Atomic Force Microscopy (AFM). Control A: bare mica (A); Control B: mica functionalised with APTES using liquid deposition technique (B); Control C: mica functionalised with APTES using vapour deposition technique (C); Control D: mica functionalised with APTES with addition of PFA:GA (3%:1.5%) fixatives using liquid deposition technique (D); Control E: mica functionalised with APTES with addition of PFA:GA (3%:1.5%) fixatives using vapour deposition technique (E). Images were obtained by Icon Dimensions (Bruker, USA), 1x1 μm in dimension.

In Table 1., the *Row/Column Statistics* and *Statistical Quantities* tools were used to calculate 2D (R_q and R_a) and 3D characteristics (S_q and S_a).

Table 1. 2D and 3D roughness characteristics. All values are depicted in nanometers. Control A: bare mica; Control B: mica functionalised with APTES using liquid deposition technique; Control C: mica functionalised with APTES using vapour deposition technique; Control D: mica functionalised with APTES with addition of PFA:GA (3%:1.5%) fixatives using liquid deposition technique; Control E: mica functionalised with APTES with addition of PFA:GA (3%:1.5%) fixatives using vapour deposition technique. Data obtained in Gwyddion editing software from surfaces depicted in Figure 16.

	R_q (RMS) /nm	S_q (RMS of height)/nm	R_a (roughness average)/nm	S_a (arithmetic mean of height)/nm
Control A	0.2764 ± 0.0645	0.2773	0.2048 ± 0.0313	0.2042
Control B	1.5330 ± 0.2778	1.5460	1.1640 ± 0.1785	1.168
Control C	0.2963 ±0.0510	0.2963	0.2287 ± 0.0273	0.2287
Control D	0.8296 ± 0.0894	0.8302	0.6684 ± 0.0625	0.6680
Control E	0.4390 ± 0.0866	0.4403	0.3378 ± 0.0388	0.3370

R_q and S_q values increased after functionalising mica with APTES, starting with R_q = 0.2764 ± 0.0645 nm and S_q = 0.2773 nm for bare mica (Control A), increasing slightly when functionalised with APTES in vapour (Control C) to R_q = 0.2963 ± 0.0510 nm and S_q = 0.2963 nm. A greater increase was noticed when mica was functionalised with APTES in liquid, Control B, (R_q = 1.5330 ± 0.2778 nm and S_q = 1.5460 nm). When fixative was added the roughness values decreased for Control D (R_q = 0.8296 ± 0.0894 nm, S_q = 0.8302 nm) and increased for Control E (R_q = 0.4390 ± 0.0866 nm, S_q = 0.4403 nm). Similar pattern can be seen in both S_a and R_a values.

4.2. Impact of Different Dehydration and Drying Methods on EV Binding and Yield

There were two methods for dehydration and drying investigated: (i) dehydration in EtOH gradient and CPD and (ii) dehydration with 2,2-DMP and drying with HMDS. Both methods were evaluated regarding functionalisation of mica with APTES applied in liquid and vapour which forms four protocols:

Protocol 1 (P1): mica functionalised with APTES using liquid deposition technique, dehydrated with EtOH and underwent CPD;

Protocol 2 (P2): mica functionalised with APTES using vapour deposition technique, dehydrated with EtOH and underwent CPD;

Protocol 3 (P3): mica functionalised with APTES using liquid deposition technique, dehydrated with 2,2-DMP and underwent drying by HMDS;

Protocol 4 (P4): mica functionalised with APTES using vapour deposition technique, dehydrated with 2,2-DMP and underwent drying by HMDS.

All protocols included fixation of EVs with PFA:GA mixture to final concentration 3%:1.5%. Two images 10x10 µm in size were analysed for particle frequency, diameter, and height data. For better resolution and view, images were resized to 5x5 µm and one representative image with 2 enlarged structures were presented. The limits for height artefact detection were taken from Control D and E, and for diameter artefact detection the lower end of the recorded EVs of the protocols were taken. Said lower limits for liquid APTES deposition protocols (P1, P3) are ≤ 0.90 nm for the diameter and ≤ 6 nm for height. For vapour APTES deposition protocols (P2, P4), lower limit for the diameter is ≤ 0.90 nm and for height ≤ 5.6 nm. Values under those lower limits were considered particles that don't represent EVs (artefacts).

4.2.1. Ethanol Dehydration With Drying at Critical Point of CO$_2$, Liquid (3-Aminopropyl)triethoxysilane Deposition (P1)

There are different shapes of EVs on the functionalised surface (Figure 17.A), most interesting representation being the round (Figure 17.B) and "cup-shaped" EVs (Figure 17.C).
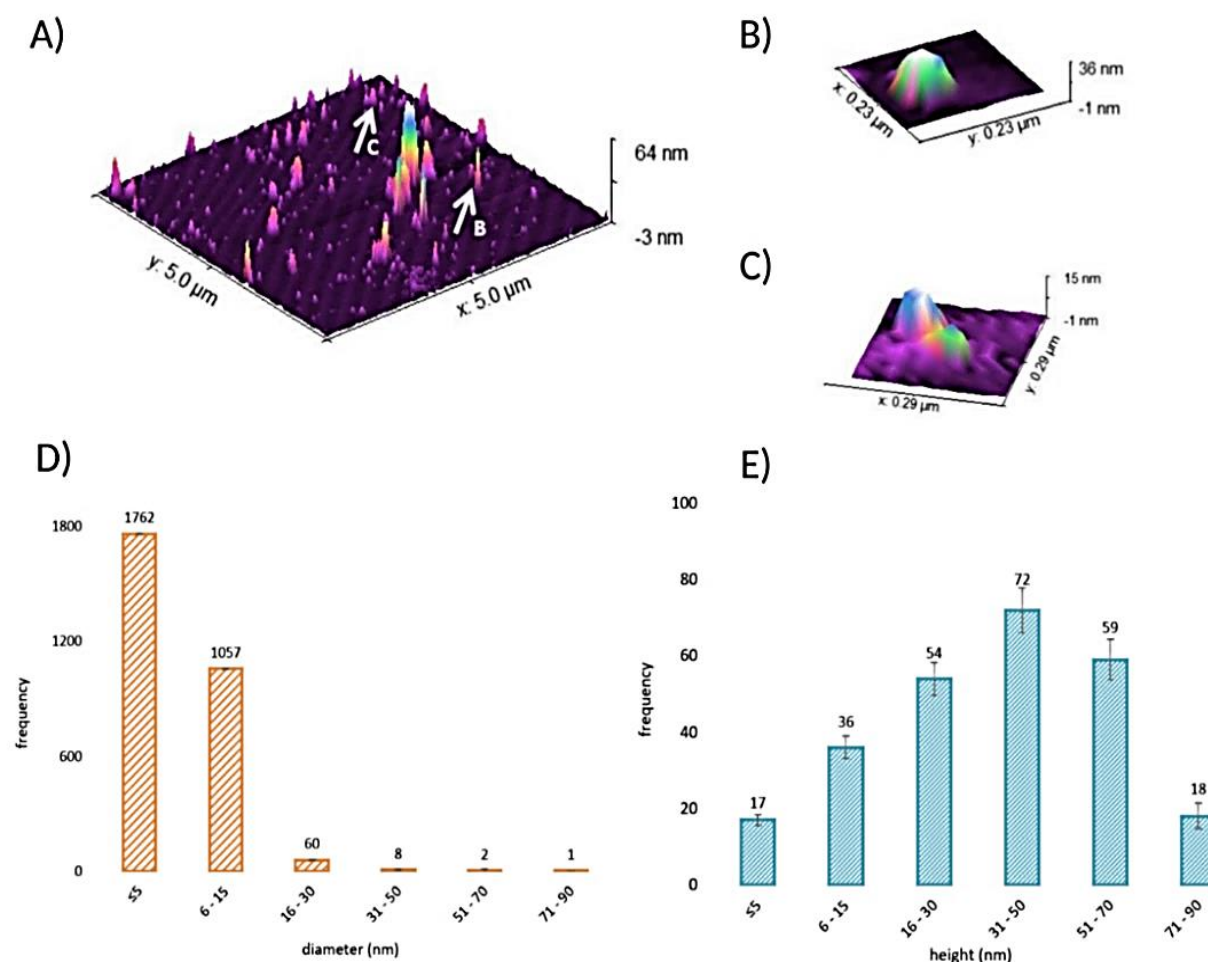
Figure 17. Mica functionalised with (3-Aminopropyl)triethoxysilane (APTES) using liquid deposition technique, dehydrated with EtOH and underwent critical point drying (CPD). 3D view of said surface, 5x5 µm in dimension (A). 3D view of round (B) and "cup-shaped" (C) EVs with a difference in structure, also marked with white arrows on (A). Distribution graphs of respective diameter (D) and height (E) of EVs in nanometers (nm) and standard deviations of intervals.

Graphs depict diameter (Figure 17.D) and height (Figure 17.E) over data frequency of the EVs. Total number of EVs captured was 2890. Most of the EVs were in ≤5 nm (N$_{EVs}$=1762) and in 6 – 15 nm (N$_{EVs}$=1057) diameter

intervals. Height graph has highest EV frequency in the 31 – 50 nm interval (N_{EVs}=72). Lowest frequency of EVs was recorded in 71 – 90 nm diameter interval (N_{EVs}=1) and ≤5 nm height interval (N_{EVs}=17). Considering the lower limits for determination of artefacts for this sample, there are 21 artefacts, all of height, of which 17 are present in the ≤5 nm interval and 4 are present in the 6 – 15 nm interval (Figure 17.E).

4.2.2. Ethanol Dehydration With Drying at Critical Point of CO_2, Vapour (3-Aminopropyl)triethoxysilane Deposition (P2)

EVs different in shape were present (Figure 18.A), including round shaped (Figure 18.B) and multilobed EVs (Figure 18.C).

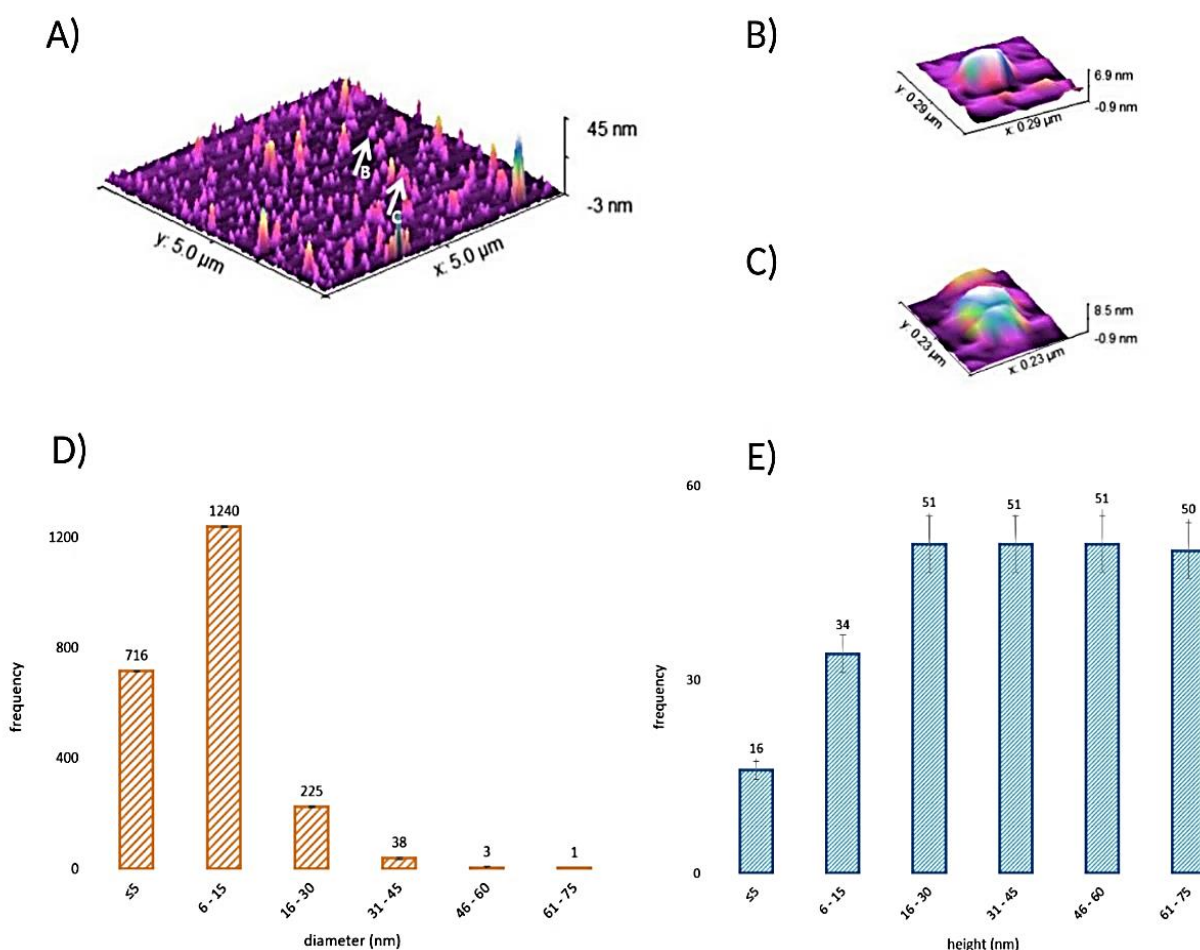**Figure 18.** Mica functionalised with APTES using vapour deposition technique, dehydrated with EtOH and underwent CPD. 3D view of said surface (A), 5x5 µm in dimension. 3D view of round (B) and multilobed (C) EVs with a difference in structure, also marked with white arrows on (A). Distribution graphs of respective diameter (D) and height (E) of EVs in nanometers (nm) and standard deviations of intervals.

Highest frequency of EVs (N_{EVs}=1240) was found within the 6 – 15 nm diameter interval with almost half the number (N_{EVs}=716) recorded in first interval (Figure 18.D). Equal number of EVs (N_{EVs}=51) were reported in the 16 – 30 nm, 31 - 45 nm and 46 - 60 nm height intervals (Figure 18.E). Lowest frequency of EVs was found in 61 – 75 nm diameter interval (N_{EVs}=1) and ≤5 nm height interval (N_{EVs}=16). Considering the limits for determination of artefacts there are 18 artefacts present, all of them in height distribution, of which 16 in the ≤5 nm interval and 2 in the 6 – 15 nm interval (Figure 18.E).

4.2.3. 2,2-Dimethoxypropane Dehydration With Hexamethyldisilazane Drying, Liquid (3-Aminopropyl)triethoxysilane Deposition (P3)

There is a different variety of EV shapes present throughout the surface (Figure 19.A), with round (Figure 19.B) and multilobed EVs (Figure 19.C) shown in enlarged perspective for a better view. EVs smaller in diameter (≤5 nm and 6 – 15 nm range) were predominantly present (Figure 19.D) with highest frequency of EVs (N_{EVs}=1205) in ≤5 nm diameter interval, whilst the highest frequency of EVs (N_{EVs}=96) was recorded in 16 – 30 nm height interval (Figure 19.E). Lowest frequency of EVs can be found in 41 – 50 nm diameter interval (N_{EVs}=0) and 51- 60 nm height interval (N_{EVs}=0). Considering the limits for determination of artefacts for this sample, there are 35 artefacts present, 31 in ≤5 nm height interval and the rest in 6 – 15 nm height interval (Figure 19.E).

Figure 19. Mica functionalised with APTES using liquid deposition technique, dehydrated with 2,2-DMP and underwent drying by HMDS. 3D view of said surface (A), 5x5 µm in dimension. 3D view of round (B) and "cup-shaped" (C) EVs, marked also with white arrows on (A). Distribution graphs of respective diameter (D) and height (E) of EVs in nanometers (nm) and standard deviations of intervals.

4.2.4. 2,2-Dimethoxypropane Dehydration With Hexamethyldisilazane Drying, Vapour (3-Aminopropyl)triethoxysilane Deposition (P4)

The shapes of the EVs were somewhat different (Figure 20.A) with the most EVs having either being perfectly round (Figure 20.B) or concave shaped, that have a collapsed lumen in the middle, reminiscent yet different than that of regular "cup-shaped" EVs (Figure 20.C).
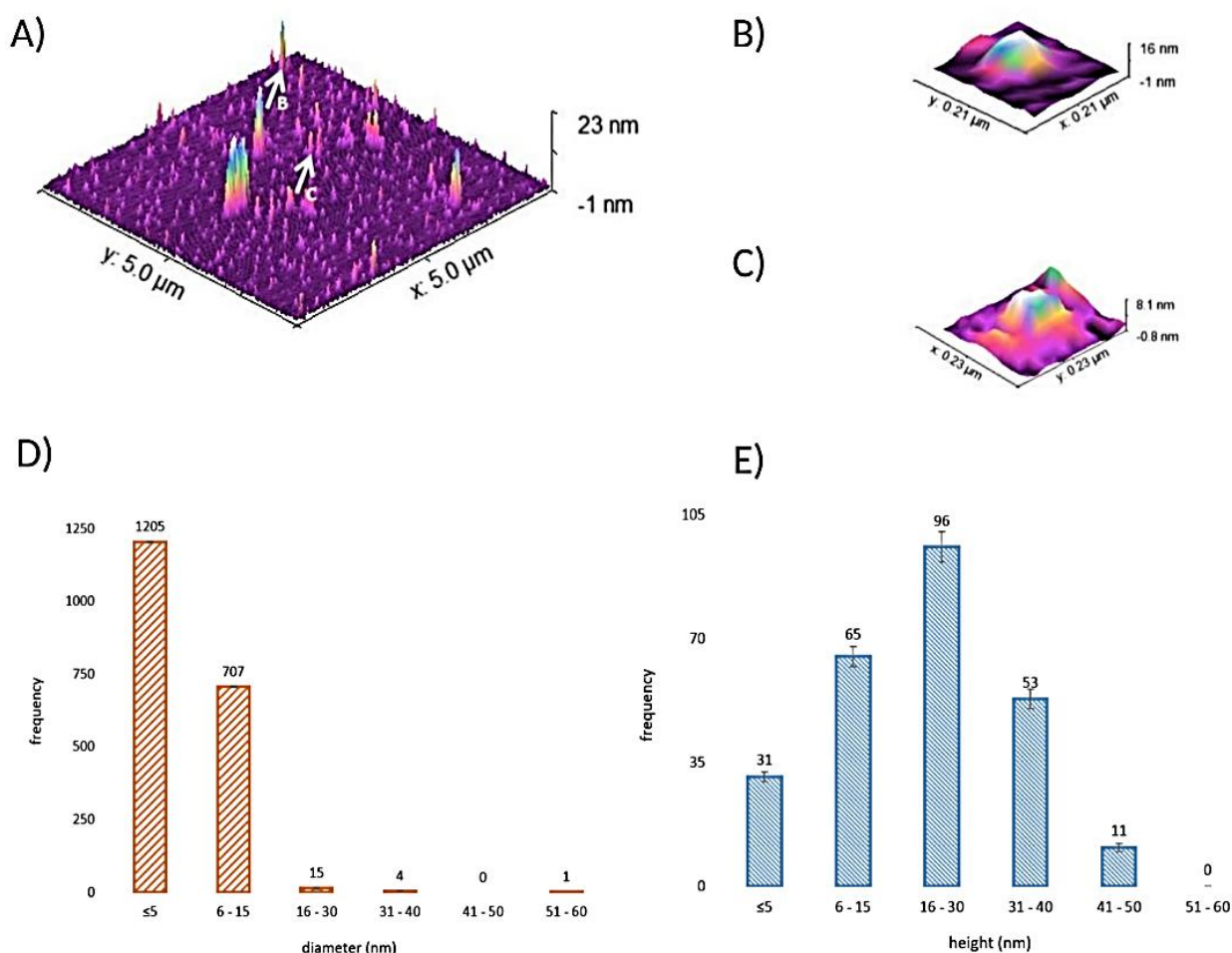
Figure 20. Mica functionalised with APTES using vapour deposition technique, dehydrated with 2,2-DMP and underwent drying by HMDS. 3D view of said surface (A), 5x5 μm in dimension. 3D view of round (B) and concave (C) EVs, significantly different in shape, marked also with white arrows on (A). Distribution graphs of respective diameter (D) and height (E) of EVs in nanometers (nm) and standard deviations of intervals.

Graphs show highest EV frequency (N_{EVs}= 891) in 6 – 15 nm diameter interval (Figure 20.D) and highest frequency of EVs (N_{EVs}=64) in 16 – 30 nm height interval (Figure 20.E), however notable are 31 – 40 nm and 41 – 50 nm height intervals with equal number of EV count (N_{EVs}=43). Lowest frequency of EVs can be found in 46 – 55 nm diameter interval (N_{EVs}=1) and ≤5 nm height interval (N_{EVs}=20). Considering the limits for

determination of artefacts for this sample there are 22 artefacts present in the height data, 2 stemming from the 6 – 15 nm height interval and the rest can be found in ≤5 nm height interval (Figure 20.E).

4.3. Statistical Comparison of EV Size and Height Distribution From Different Sample Preparation Protocols

To determine which protocol and technique performed the best and is the optimal to use for further research, Origin Software was used to compare results in several different ways. After removing the artefacts out of the data, descriptive statistics was performed for diameter (Table 2.) and height values (Table 3.).

Table 2. Descriptive statistics results of diameter data after ruling out the artefact values.

Protocol	N_{EVs}	Median/nm	Range (Minimum - Maximum)/nm
P1	2890	4.95	0.90 – 85.01
P2	2223	8.02	0.90 – 62.65
P3	1932	4.27	2.90 – 57.19
P4	1506	10.58	2.90 – 51.89

Legend: P1 (Protocol 1) - mica functionalised with APTES using liquid deposition technique, dehydrated with EtOH and underwent CPD; P2 (Protocol 2) - mica functionalised with APTES using vapour deposition technique, dehydrated with EtOH and underwent CPD; P3 (Protocol 3) - mica functionalised with APTES using liquid deposi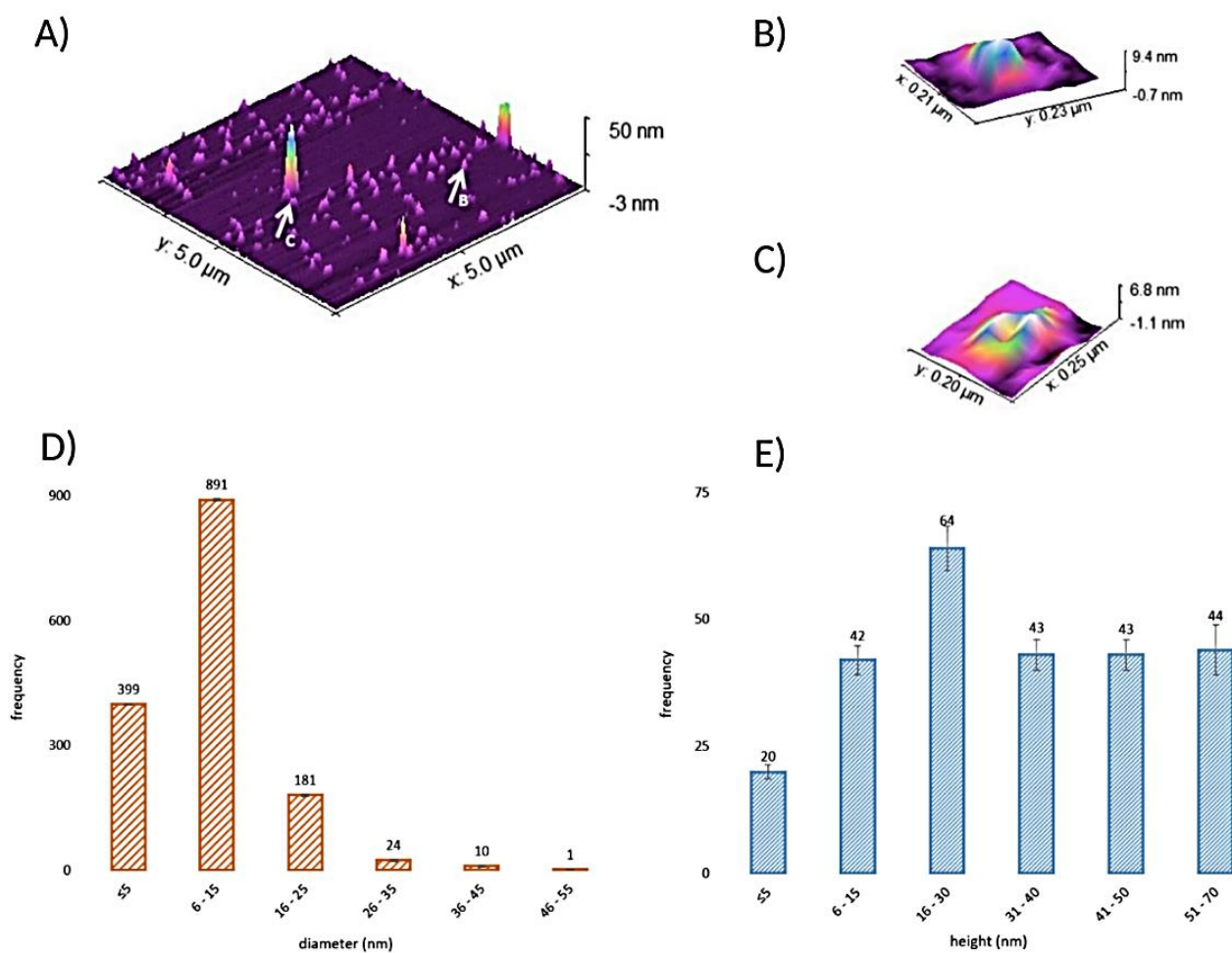tion technique, dehydrated with 2,2-DMP and underwent drying by HMDS; P4 (Protocol 4) - mica functionalised with APTES using vapour deposition technique, dehydrated with 2,2-DMP and underwent drying by HMDS.

Table 3. Descriptive statistics results of the height data after ruling out the artefact values.

Protocol	N_{EVs}	Median/nm	Range (Minimum-Maximum)/nm
P1	235	38.66	6.33 – 80.99
P2	238	40.58	5.79 – 76.31
P3	219	22.90	6.02 – 43.60
P4	233	33.14	5.69 – 66.28

Legend: P1 (Protocol 1) - mica functionalised with APTES using liquid deposition technique, dehydrated with EtOH and underwent CPD; P2 (Protocol 2) - mica functionalised with APTES using vapour deposition technique, dehydrated with EtOH and underwent CPD; P3 (Protocol 3) - mica functionalised with APTES using liquid deposition technique, dehydrated with 2,2-DMP and underwent drying by HMDS; P4 (Protocol 4) - mica functionalised with APTES using vapour deposition technique, dehydrated with 2,2-DMP and underwent drying by HMDS.

In Table 2., P1 shows biggest diameter value range (0.90 nm – 85.01 nm), highest N total of the EVs (N_{EVs}) recorded (2980), whereas P4 shows the smallest diameter value range (2.90 nm – 51. 89 nm) and lowest frequency of EVs (N_{EVs}=1506). Notably, P3 has the lowest median value (4.27 nm) whilst P4 has the highest median value out of all protocols (10.58 nm). Table 3. shows similar results, with P1 having the highest height range (6.33 nm – 80.99 nm). P3 has the lowest height range (6.02 nm – 43.60 nm).

Following the descriptive analysis, a Kolmogorov-Smirnov normality test (significance level: α=0.05) was performed. Diameter data of each protocol revealed that none of the protocols have normal diameter data distribution, therefore it was proceeded with a nonparametric test. Height data showed normal distribution with the normality test in all of the protocols, so it was proceeded with a parametric test. Kruskal-Wallis H-test, used on diameter values, compares the means of four protocols in order to determine whether there is statistical evidence that the associated means are significantly different in any way. The results of the test show that P4 has the highest diameter mean (10.33 nm), followed by P2 (8.83 nm) with P1 (5.62 nm) on the lower end and P3 with the lowest diameter mean (5.35 nm) (Table 2., Figure 21.A). Origin was used to calculate standard deviation (SD) of diameter for each protocol (Figure 21.A). P2 has the highest SD (6.61 nm), followed by P4 (5.99 nm), P1 (4.11 nm) and lastly, P3 (2.67 nm). Diameter range within 1.5 interquartile (IQR) was also computed, along with the outliers (Figure 21.B). P4 has the widest diameter range (4.95 – 13.8 nm) and P1 the narrowest diameter range (2.90 – 6.66 nm). The highest frequency of outliers can be found in P1 (121) and P2 (110). P4 has the lowest outlier frequency (26). Post-hoc Mann-Whitney U-test was used to compare the diameter values to determine if there's any significant differences between the samples.
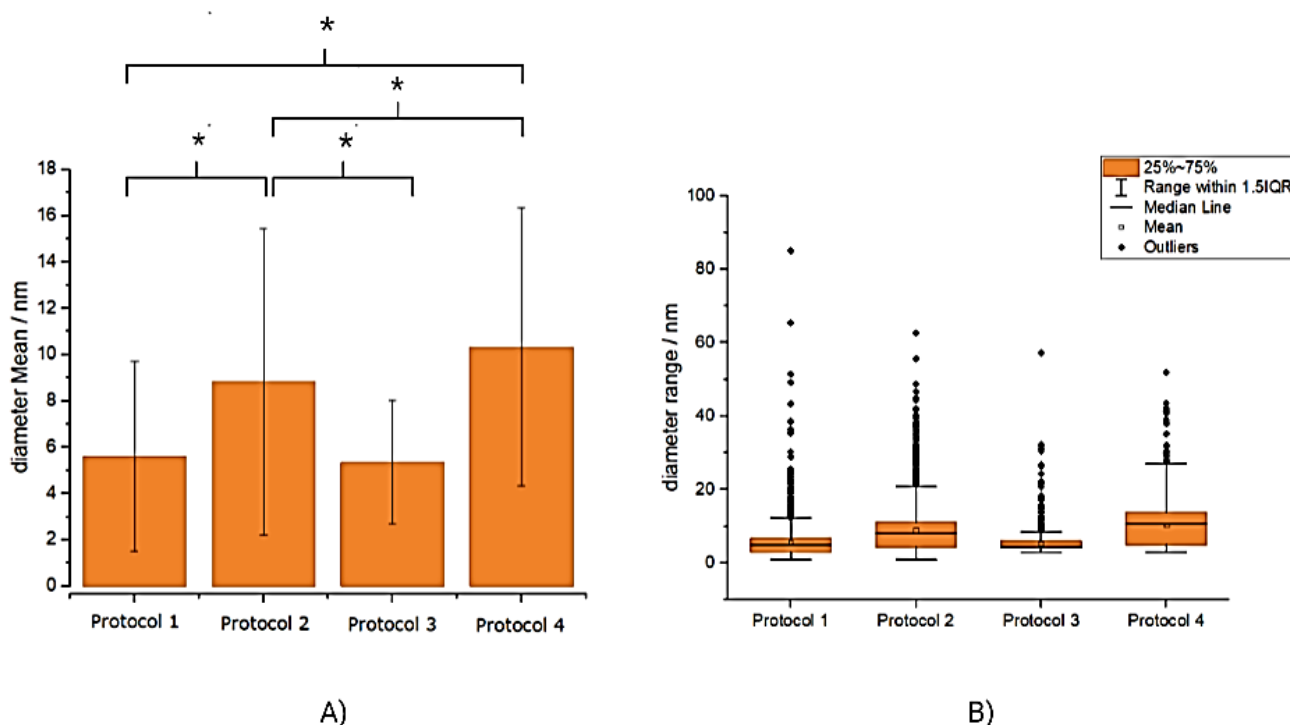
Figure 21. Extracellular vesicle (EV) diameter mean values (in nm) after four different treatment protocols, captured by atomic force microscopy (AFM), and computed in Origin Software. Graphic comparison of EV diameters according to samples of the treatment (bar format) with respective standard deviations (line format) (A). Kruskal-Wallis' H-test with post-hoc Mann-Whitney U-test was used to show significant difference between the samples, with significance level of *<0.05; Graphic representation of EV diameter range for each sample in a form of vertical box-whisker plots (B). Shown are median lines with mean as a square in each box with the corresponding interquartile range (IQR). The box height corresponds to the IQR, the lines extending from the box indicate variability outside the IQR (range within the 1.5IQR). Outliers (values outside of the range) are indicated as black squares.

Origin was further used for statistical analysis of EV height data. The results of the parametric ANOVA test show that out of four protocols, P2 has the highest height mean value (40.57 nm), closely followed by P1 (39.36 nm). P4 has height mean value of 33.31 nm whilst the lowest is the height mean value for P3 (23.13 nm) (Figure 22.A). SD was also calculated – highest SD value is that of P2 (20.25 nm), followed by P1 (19.89 nm), P4 (16.33 nm) and lastly P3 (10.16 nm). Software also calculated height range within IQR for each method. P1 has the greatest height range (6.32 – 80.99 nm), followed by P2 (5.79 nm – 76.31 nm), P4 (5.69 – 66.28 nm) and lastly P3

(6.02 – 43.60 nm). No outliers were found outside of the 1.5IQR (Figure 22.B).

A)

B)
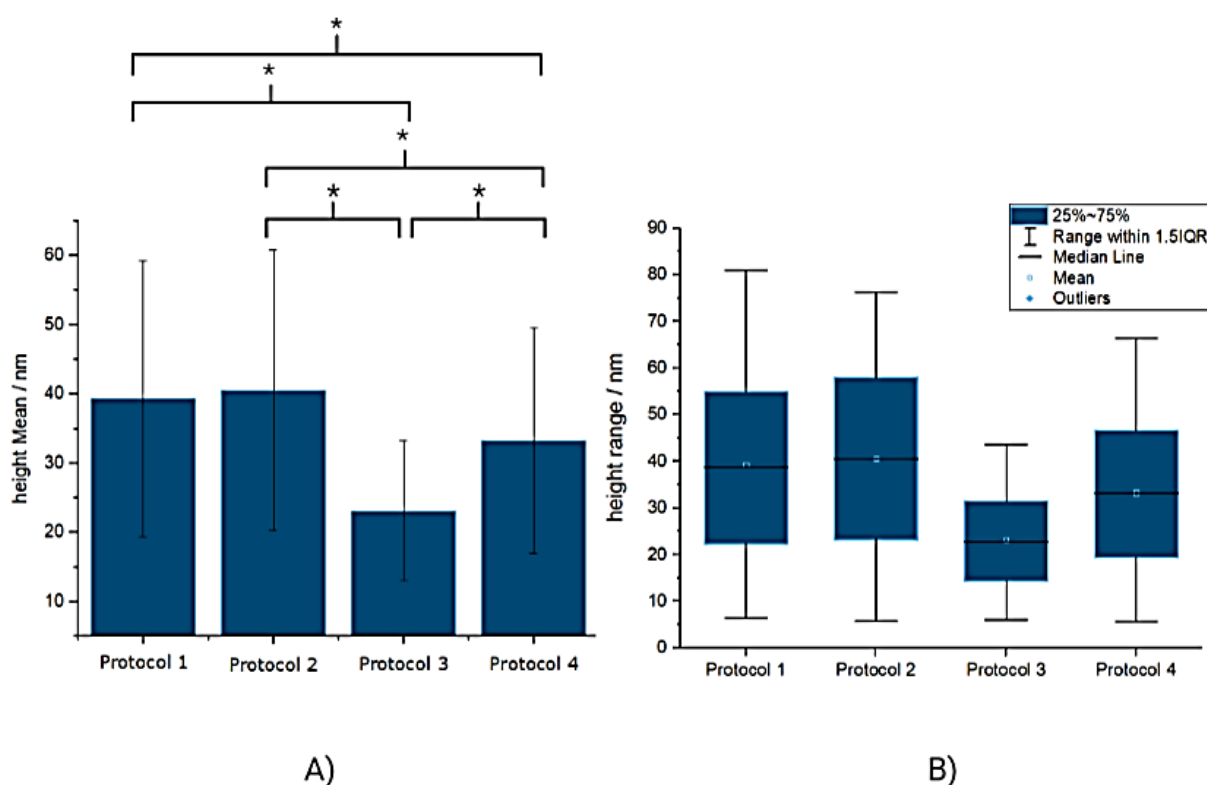
Figure 22. Extracellular vesicle (EV) height mean values (in nm) after four different treatment methods, captured by atomic force microscopy (AFM), and computed in Origin Software. Graphic comparison of EV height according to samples of treatments (bar format) with respective standard deviations (line format) (A). ANOVA test with post-hoc Mann-Whitney U-test was used to show significant difference between the samples, with significance level of *<0.05; Graphic representation of EV height range for each sample in a form of vertical box-whisker plots (B). Shown are median lines with mean as a square in each box with the corresponding interquartile range (IQR). The box height corresponds to the IQR, the lines extending from the box indicate variability outside the IQR (range within the 1.5IQR). Outliers (values outside of the range) are indicated as black squares.

5. DISCUSSION

Nowadays, EVs are known for their transport role in cell-to-cell communication where they deliver cargo from donor to recipient cells and modulate their physiological condition. They contain a plethora of protein, nucleic acid, lipid cargoes and play roles in multiple signalling pathways (30). Because of their ever-growing link to physiological and pathological processes, interest in EVs has been and still is exponentially growing (31). The new field of EV research, however, has many obstacles when it comes to isolation, identification, and quantification as well as downstream analysis of EVs, which makes it difficult to correctly attribute the biological effects connected to the physiological or pathological conditions. Scientific community recognises the need to standardise the methodology and technology (31), with International Society of Extracellular Vesicles (ISEV) taking the lead role in promoting the advance in techniques and procedures. This work explored four different types of protocols for EV visualisation by AFM in air, and how different APTES functionalisation techniques influence surface roughness values and effects on EV binding. Focus was also on comparison of EV size and height throughout the protocols and ultimately which protocol gives better EV yield.

First step of the experiment was to functionalise mica crystal with APTES, which was done by liquid or vapour deposition. This was done to improve the surface potential of mica to better bind the EVs to its surface. Before introducing the samples onto the surface, controls were made separately to compare 2D and 3D surface roughness parameters between different deposition techniques (Table 1.) as well as compare them to the available literature values. Bare mica (Control A) had the lowest values out of all others (R_q = 0.2764 ± 0.0645 nm, S_q = 0.2773 nm, R_a = 0.2048 ± 0.0313 nm, S_a = 0.2042) which agrees with the literature data (32). Compared to the rest, mica functionalised with APTES using vapour deposition (Control C) has the lowest roughness values (R_q = 0.2963 ±0.0510 nm, S_q = 0.2963 nm, R_a = 0.2287 ± 0.0273 nm, S_a = 0.2287) which agrees with the

literature value of $R_q=0.2000$ nm (33). When comparing the literature values ($R_q = 0.1800 \pm 0.0300$ nm and $R_q=0.2100 \pm 0.0300$ nm) of mica functionalised with APTES using liquid deposition (Control B) (14) to the experimental roughness value of Control B ($R_q = 1.5330 \pm 0.2778$ nm), the values are significantly lower. The difference when comparing experimental and literature values might've occurred due to technical differences since there's no standardised method. Same thing happened with mica functionalised with APTES with addition of PFA:GA fixatives using liquid (Control D) and vapour deposition (Control E), with former having higher roughness values ($R_q = 0.8296 \pm 0.0894$ nm, $S_q = 0.8302$ nm, $R_a = 0.6684 \pm 0.0625$ nm, $S_a = 0.6680$) than the latter ($R_q = 0.4390 \pm 0.0866$ nm, $S_q= 0.4403$nm, $R_a = 0.3378 \pm 0.0388$ nm, $S_a = 0.3370$). The results confirm that the vapour deposition technique, which is performed in a desiccator without water contact (See *Section 3.2.3.*), manages to produce a smoother surface.

For the next part, samples were deposited onto four functionalised mica crystals that then followed four different protocols – P1: liquid APTES functionalisation with EtOH dehydration and CPD, P2: vapour APTES functionalisation with EtOH dehydration and CPD, P3: liquid APTES functionalisation with 2,2-DMP dehydration and HMDS drying, and P4: vapour APTES functionalisation with 2,2-DMP dehydration and HMDS drying. All of the protocols have shown good EV adherence to mica surface functionalised with APTES. When searching for EVs, different shapes present were annotated, most commonly: round, "cup-shaped", multilobed and concave. It's notable that P1 and P2 (Figure 17. and 18.) produced a rougher, more irregular surface when compared to P3 and P4 (Figure 19. and 20.). Irregularities can be explained as precipitated salts from phosphate buffer (used as a mobile phase in the isolation of EVs by size-exclusion chromatography). Kruskal-Wallis H-test indicated that at $p < 0.05$, diameter means of all protocols are significantly different. To compare the diameter values between all the protocols, post-hoc Mann-Whitney U-

test was performed. With the significance level of $p < 0.05$, the test has shown significant difference between all of the protocols but not P1 and P3 ($p = 0.14$) (Figure 21.A). Looking at the height values, parametric one-way ANOVA ($p < 0.05$) indicated significant difference between height mean values of the protocols and post-hoc Mann-Whitney U-test ($p < 0.05$) has shown significant difference between all of the protocols except P1 and P2 ($p = 0.48$) (Figure 22.A).

Selection of the most appropriate protocol was based on multiple factors: diameter and height mean, median and range values, SD, outlier count, but mostly on overlaps of total number of detected EVs (N_{EVs}) of diameter and height. P4 shows the best overlap of N_{EVs} in diameter ($N_{EVs}=1506$, 0 artefacts) and height ($N_{EVs}=233$, 22 artefacts), highest diameter median (10.58 nm) and mean value (10.33 ± 5.99 nm), and lowest number of diameter outliers (26) out of all other protocols. SD range is acceptable in both diameter (5.99 nm) and height (16.33 nm). All of these statistics agree with literature EV diameter and height values that have been reported in both AFM air and liquid (2,8,34). Next best protocol, P2, shows third best overlap of N_{EVs} in diameter (2223) and height (238) with the least artefacts (18, all height value artefacts) out of all protocols, highest height median (40.58 nm), second highest diameter mean (8.83 ± 6.61 nm), highest height mean (40.57 ± 20.25 nm). Protocols P1 and P3 do not show concordance in overlaps of EV diameter and height, neither can they compare with statistical values of P4 and P2. It's important to note that both P2 and P4 APTES functionalisation was performed via vapour technique. Ultimately, statistical data points toward P4 as the most optimal protocol out of all others for preparation of EVs and AFM air mode visualisation.

In this work, criteria for EV selection were based on shape, size, diameter, and height values. When choosing the protocols, it was important to opt for different types of dehydration and drying technique combinations. Here, two types of drying techniques were used – CPD, which has been proven

to preserve the shape and structure of EVs, and HMDS drying which has proven to be an equally good alternative, with easier implementation and the same amount of shrinkage of the sample when compared to CPD (12,21). To conclude, AFM is a promising, powerful technique that should be implemented more often for it to gain its full potential, especially in EV research and morphology analysis. In the future, researchers should use proved techniques, and whilst continuing to develop and build upon those also experiment with new ones so that EVs from CSF (and other bodily fluids) can develop to be functional novel biomarkers for diagnosis, treatment, and disease prognostics.

6. CONCLUSION

The optimal sample preparation protocol for EV visualisation by AFM in air (intermittent tapping mode) is the one that involves fixation by PFA:GA, vapour APTES functionalisation of mica crystal, dehydration with 2,2-DMP and HMDS drying.

Through control surfaces and their roughness values, and four protocols and their statistical factors, it has been noted that vapour APTES functionalisation shows more even distribution of APTES on mica crystal when compared to liquid APTES functionalisation. Also, it gives a smoother surface overall, which in turn improves EV visualisation in AFM air and gives less artefacts.

AFM, which is a very sensitive nanotechnology, identified EVs of different shapes and sizes, with most common shapes being round, multilobed, "cup-shaped" and concave. For this type of analysis, lower limit for detection of artefacts by AFM gave only a small number of artefacts, which means that for future analysis higher limit should be taken up to eliminate potential small particles that come from phosphate buffer.

Limiting factor of this research is the inability to separate EVs from other particles of the same size by size-exclusion chromatography in the early stages of research. Since this factor was not the primary focus of the work, future research should focus on eliminating this problem by using methods and techniques such as immuno-based detection, that uses EV antigen and antibody interaction to detect and differentiate EVs from others.

7. REFERENCES

1. Parisse P, Rago I, Ulloa Severino L, Perissinotto F, Ambrosetti E, Paoletti P, et al. Atomic force microscopy analysis of extracellular vesicles. Eur Biophys J. 2017;46(8):813–20.

2. Malenica M, Vukomanović M, Kurtjak M, Masciotti V, dal Zilio S, Greco S, et al. Perspectives of Microscopy Methods for Morphology Characterisation of Extracellular Vesicles from Human Biofluids. Biomedicines [Internet]. 2021 May 26;9(6):603. Available from: https://www.mdpi.com/2227-9059/9/6/603

3. Gazze SA, Thomas SJ, Garcia-Parra J, James DW, Rees P, Marsh-Durban V, et al. High content, quantitative AFM analysis of the scalable biomechanical properties of extracellular vesicles. Nanoscale. 2021;13(12):6129–41.

4. Cavallaro S, Pevere F, Stridfeldt F, Görgens A, Paba C, Sahu SS, et al. Multiparametric Profiling of Single Nanoscale Extracellular Vesicles by Combined Atomic Force and Fluorescence Microscopy: Correlation and Heterogeneity in Their Molecular and Biophysical Features. Small. 2021;17(14).

5. Iwai K, Minamisawa T, Suga K, Yajima Y, Shiba K. Isolation of human salivary extracellular vesicles by iodixanol density gradient ultracentrifugation and their characterizations. J Extracell Vesicles. 2016;5(1).

6. BioRender. Image and template manager [Internet]. 2022. Available from: https://app.biorender.com/biorender-templates.

7. NanoAndMore GMBH [Internet]. What is Atomic Force Microscopy (AFM). Available from: https://www.nanoandmore.com/what-is-atomic-force-microscopy

8. Vidović I. Application of nanotechnologies for quantification measurement of nanoparticles from human cerebrospinal fluid : comparison of atomic force microscopy and tunable resistive pulse sensing [Internet]. University of Rijeka; 2021. Available from: https://urn.nsk.hr/urn:nbn:hr:193:956840

9. University of Cambridge. Atomic Force Microscopy - Modes of Operation [Internet]. Modes of Operation. 2022. Available from: https://www.doitpoms.ac.uk/tlplib/afm/modes_operation.php

10. Park Systems. Contact mode [Internet]. 2022. p. 4. Available from: https://www.parksystems.com/park-spm-modes/91-standard-imaging-mode/223-basic-contact-afm-dynamic-force-microscope-dfm

11. Baričević V. Protocol optimisation for the visualisation of extracellular vesicles from cerebrospinal fluid of patients with traumatic brain injury on scanning electron microscope [Internet]. University of Rijeka; 2021. Available from: https://urn.nsk.hr/urn:nbn:hr:193:937728

12. Qin Y, Jiang W, Li A, Gao M, Liu H, Gao Y, et al. The Combination of Paraformaldehyde and Glutaraldehyde Is a Potential Fixative for Mitochondria. Biomolecules [Internet]. 2021 May 10;11(5):711. Available from: https://www.mdpi.com/2218-273X/11/5/711

13. Fire Mountain Gems and Beads®. Gem Notes: Gemstone Information - Mica Meaning and Properties [Internet]. 2022. Available from: https://www.firemountaingems.com/resources/encyclobeadia/gem-notes/hc0l

14. Zapletalová H, Malohlava J, Tománková K, Kolářová H. Analysis of Functionalized Mica Substrates for Afm Imaging of Dna. 2012;2012.

15. Shlyakhtenko LS, Gall AA, Filonov A, Cerovac Z, Lushnikov A, Lyubchenko YL. Silatrane-based surface chemistry for immobilization of DNA, protein-DNA

complexes and other biological materials. Ultramicroscopy [Internet]. 2003 Oct;97(1–4):279–87. Available from: https://linkinghub.elsevier.com/retrieve/pii/S0304399103000536

16. Crampton N, Bonass WA, Kirkham J, Thomson NH. Formation of aminosilane-functionalized mica for atomic force microscopy imaging of DNA. Langmuir. 2005;21(17):7884–91.

17. Watté J. Low Temperature Deposition of Photocatalytically Active TiO 2 Coatings on Polymers. 2017;(January).

18. Facult LA. Quasistatic and Dynamic Force Microscopy of Single Antigen-Antibody Complexes and Fibrin-Fibrinogen Systems. 2004;2946.

19. Electron Microscopy Sciences. Critical Point Drying Principles [Internet]. 2021. Available from: https://www.emsdiasum.com/microscopy/technical/datasheet/critical_drying.aspx

20. Grillet N. High-resolution imaging of the mouse-hair-cell hair bundle by scanning electron microscopy. STAR Protoc [Internet]. 2022;3(1):101213. Available from: https://doi.org/10.1016/j.xpro.2022.101213

21. Braet F, De Zanger R, Wisse E. Drying cells for SEM, AFM and TEM by hexamethyldisilazane: A study on hepatic endothelial cells. Vol. 186, Journal of Microscopy. 1997. p. 84–7.

22. Roth C. 1,1,1,3,3,3-Hexamethyldisilazane (HMDS), 250 ml ≥98 %, for the GC [Internet]. 2022 [cited 2022 Aug 28]. p. 1. Available from: https://www.carlroth.com/at/en/reagents-for-silylation/111333-hexamethyldisilazane-%28hmds%29/p/3840.2

23. University of Kentucky College of Medicine. Neurosurgery - Ventriculostomy [Internet]. 2022. Available from: https://neurosurgery.med.uky.edu/neurosurgery-ventriculostomy#:~:text=Ventriculostomy is also called ventricular,to an external collecting device.

24. Berktas I, Ghafar AN, Fontana P, Caputcu A, Menceloglu Y, Okan BS. Facile synthesis of graphene from waste tire/silica hybrid additives and optimization study for the fabrication of thermally enhanced cement grouts. Molecules. 2020;25(4).

25. Uchihashi T, Watanabe H, Kodera N. Chapter 10. 2018;1814:159–79.

26. Bronder AM, Bieker A. Supplemental Information Oriented Membrane Protein Reconstitution into Tethered Lipid Mem- branes for AFM Force Spectroscopy. 111.

27. Nečas D, Klapetek P. Gwyddion: An open-source software for SPM data analysis. Cent Eur J Phys. 2012;10(1):181–8.

28. Skliar M, Chernyshev VS. Imaging of extracellular vesicles by atomic force microscopy. J Vis Exp. 2019;2019(151):1–13.

29. Upmold. Ra & Rz Roughness Specification [Internet]. 2017. Available from: https://upmold.com/surface-finish-ra-rz/

30. Rybak K, Robatzek S. Functions of Extracellular Vesicles in Immunity and Virulence. Plant Physiol [Internet]. 2019 Apr;179(4):1236–47. Available from: https://academic.oup.com/plphys/article/179/4/1236-1247/6116494

31. Coumans FAW, Brisson AR, Buzas EI, Dignat-George F, Drees EEE, El-Andaloussi S, et al. Methodological Guidelines to Study Extracellular Vesicles. Circ Res

[Internet]. 2017 May 12;120(10):1632–48. Available from: https://www.ahajournals.org/doi/10.1161/CIRCRESAHA.117.309417

32. Sabihah ZN, Azlan AA, Dyana ZN. Functionalization Of Mica Surface Using Poly-L-Lysine (Pll). In: Multidisciplinary Research as Agent of Change for Industrial Revolution 40 [Internet]. 2020. p. 677–82. Available from: https://www.europeanproceedings.com/article/10.15405/epsbs.2020.03.03.79

33. Lu Q, Wang J, Faghihnejad A, Zeng H, Liu Y. Understanding the molecular interactions of lipopolysaccharides during E. coli initial adhesion with a surface forces apparatus. Soft Matter [Internet]. 2011;7(19):9366. Available from: https://pubs.rsc.org/en/content/articlelanding/2011/SM/c1sm05554b

34. Fu P, Zhang J, Li H, Mak M, Xu W, Tao Z. Extracellular vesicles as delivery systems at nano-/micro-scale. Adv Drug Deliv Rev [Internet]. 2021 Dec;179:113910. Available from: https://linkinghub.elsevier.com/retrieve/pii/S0169409X21003033

8. CURRICULUM VITAE

Ana Svetić

Date of Birth: 14/04/1999, Nationality: Croatian, Gender: Female, Contact: (+385) 0919286945

anasvetic1999@gmail.com   Nova Krasa 18, Novi Vinodolski, 51250, Croatia

WORK EXPERIENCE

01/09/2021 – CURRENT – Rijeka, Croatia

CENTER FOR -MICRO AND -NANO SCIENCES AND TECHNOLOGIES, NANORI – ASSOC. PROF. MLADENKA MALENICA and DR. MARKO PERČIĆ

Working on research project greenlighted by University of Rijeka „Uspostava protokola na Sveučilištu u Rijeci za primijenu nanotehnoloških metoda: mikroskopije atomskih sila i skenirajućeg elektronskog mikoroskopa prilikom vizualizacije i karakterizacije egzosoma"/ "Establishing a protocol at the University of Rijeka for the application of nanotechnological methods: Atomic Force Microscopy and Scanning Electron Microscopy during visualising and characterizing exosomes".

Tasks include preparing samples for analysis, statistical analysis in Gwyddion, Microsoft Excel and Origin Software. https://nanori.uniri.hr/lpemnt/hr/ Radmile Matejčić, 2, 51000, Rijeka

03/03/2022 – 15/04/2022 – Rijeka, Croatia

LABORATORY ASSISTANT FOR STUDENT LEARNING FOR "GENERAL CHEMISTRY" – UNIVERSITY OF RIJEKA, DEPARTMENT OF BIOTECHNOLOGY

Helping students understand the experiments, preparing solutions and organising laboratory practice.

09/12/2021 – 09/01/2022 – Rijeka, Croatia

LABORATORY ASSISTANT FOR STUDENT LEARNING FOR "GENERAL AND INORGANIC CHEMISTRY" – UNIVERSITY OF RIJEKA, FACULTY OF MEDICINE (MEDRI)

Helping students understand the experiments, preparing solutions and organising laboratory practice.

Rijeka, Croatia

COMPULSORY PRACTICE – TEACHING INSTITUTE FOR PUBLIC HEALTH OF THE PRIMORJE-GORSKI KOTAR COUNTY (NZZJZ)

EDUCATION AND TRAINING

20/09/2021 – CURRENT –Radmile Matejčić2, Rijeka, Croatia

MASTER OF BIOTECHNOLOGY IN MEDICINE, MAG. BIOTECH. IN MED. – University of Rijeka, Department of Biotechnology

https://www.biotech.uniri.hr/en/

01/09/2017 – 16/09/2020 –Radmile Matejčić2, Rijeka, Croatia

UNIVERSITY BACHELOR OF BIOTECHNOLOGY AND DRUG RESEARCH, UNIV. BACC. BIOTECH. ET. PHARM. INV. – Uni

University of Rijeka, Department of Biotechnology

http://gimnazija-klasicna-salezijanska-ri.skole.hr/

01/09/2013 – 02/06/2017 – Vukovarska ul. 62, Rijeka, Croatia

HIGH SCHOOL EDUCATION – Salesian Classical Gymnasium

HONOURS AND AWARDS

2021

2nd place Kendo National Championship – Croatian Kendo Association

Kyu category

2019

2nd place Kendo National Championship – Croatian Kendo Association

Scholarship of the city of Novi Vinodolski – Novi Vinodolski municipality

LANGUAGE SKILLS

Mother tongue(s): CROATIAN

Other language(s):

	UNDERSTANDING		SPEAKING		WRITING
	Listening	Reading	Spoken production	Spoken interaction	

ENGLISH	C2	C1	C2	C2	C2
GERMAN	B1	B1	A2	A2	A2

Levels: A1 and A2: Basic user; B1 and B2: Independent user; C1 and C2: Proficient user

DIGITAL SKILLS

My Digital Skills

SOCIAL MEDIA

Social Media (Facebook, Twitter, Instagram, LinkedIn), Youtube

STATISTICS

OriginPro(basic), Microsoft, Microsoft Word, Microsoft PowePoint, Microsoft Excel, Microsoft Outlook, GraphPad Statistics, Medcalc

OTHER

PyMOL, Avogadro, ChemAxon, Marvin, VMD, GAMESS, MacMOLPlt, KinTek, GROMACS

VOLUNTEERING

01/12/2021 – 23/12/2021

Kuglice dobrih želja / Balls of good wishes, Rijeka

HOBBIES AND INTERESTS

Kendo at Kendo Club Rijeka

Japanese martial arts

STUDENT WORK

01/07/2019 – CURRENT

Waitress